Supported Metal Single-Atom Thermocatalysts for Oxidation Reactions

L. Piccolo, S. Loridant, Phillip Christopher

Supported metal single-atom thermocatalysts for oxidation reactions

By Laurent Piccolo, Stéphane Loridant, and Phillip Christopher*

Affiliations

Dr. L. Piccolo, Dr. S. Loridant, IRCELYON, University of Lyon, Villeurbanne (France)

Dr. P. Christopher, Department of Chemical Engineering, University of California, Santa Barbara (USA)

Keywords: Single-atom catalysts, heterogeneous thermocatalysis, oxidation reactions, CO oxidation, PROX, water-gas shift, transition-metal oxides

Abstract: The interest in single-metal-atom dispersion in heterogeneous catalysis has existed since the 1950s with spectroscopic investigations of rhodium "single-site" catalysts supported on alumina, and more recently with oxometallate monomers for selective oxidation reactions. A decade ago, advances in electron microscopy intensified the interest of the catalysis community in controlling the dispersion of supported metals down to the single-atom active site level and revealing their intrinsic catalytic properties. Pioneering works in the ever-growing field of single-atom catalysis investigated late transition metals (group 8 to 11) supported on transition metal oxides for the CO oxidation and water-gas shift reactions. Since then, various single-atom catalysts, most often supported on oxides, have been evaluated in a broad panel of thermal oxidation reactions, and have often shown remarkable performances. Besides CO oxidation over oxide-supported noble metals, which represents the major part of the literature, this chapter reviews the main classes of oxidation reactions, including total and selective oxidations of hydrocarbons and oxygenates, on

oxide- or carbon-supported catalysts. Throughout the chapter, we emphasize several aspects that we consider important, such as the coordination environment and stability of single metal atoms, as well as their compared performance with supported nanoparticles.

1. Introduction

Single-atom catalysts (SAC) have been the subject of intense and increasing interest for a decade [1–11]. They generally differ from so-called "single-site heterogeneous catalysts" or heterogenized homogeneous catalysts – typically mononuclear metal complexes grafted on silica – since they avoid or at least minimize the use of labile organic ligands [12–14]. By design, metal atoms in SAC coordinate to atoms of solid supports or hosts [2]. Beyond nanocatalysis, the current fascination for SAC in materials research parallels a significant advance in the exploration of the subnanometric world. With respect to conventional supported catalysts, SAC provide both metal cost savings (especially interesting in the case of noble metals) and potential for novel catalytic properties owing to unique active-site electronic structure. In particular, SAC provide the potential to cumulate the site-specific selectivity of homogeneous catalysts and the advantages of heterogeneous catalysts, *i.e.* their easy handling and recovery [2].

Since the 1950s, there have been a number of early reports on heterogeneous catalysis by supported single metal atoms, identified mostly by spectroscopic characterization, *e.g.* for noble metals on Al_2O_3 [15–17], MgO [18–20], CeO_2 [21–23], and ZrO_2 [24], as well as for early transition metals anchored on SiO_2 and other oxides [12]. From the 2011 paper by Zhang and coworkers [25], the term "single atoms" (SA) has been widely used, especially for late transition metals, whereas equivalent terms such as "isolated" and "individually dispersed" metal atoms or species, as well as "single sites" and "mononuclear species", were previously preferred – and are sometimes still in use (the term "atomically dispersed" is also frequently employed, but this may also cover e.g. 2D raft-like or subnanometric 3D clusters [26]).

Though conventional heterogeneous metal-based catalysts often contain SA in addition to clusters and nanoparticles (NP) [1], it is only recently that atomic dispersion of the metal can be accurately controlled and assessed, in particular through visualization by aberration-

corrected scanning transmission electron microscopy (aberration-corrected STEM) [27]. The possibility to "see" individual atoms has stimulated research into synthesis, characterization, and reactivity of SAC, especially for late transition metal atoms on oxide supports. The pioneering works on so-identified SAC in the early 2010s were devoted to noble metal atoms supported on high-surface-area metal oxides, with CO oxidation (in absence or presence of hydrogen) [25,28] or water-gas shift (WGS) [29,30] as the main test-reactions. Since then, the scope of SAC has considerably expanded to all domains of heterogeneous catalysis, including electrocatalysis and photocatalysis, in parallel to the increasing use of non-noble metals and carbon/nitrogen-containing hosts. Regarding thermal oxidation reactions, noble metals supported on oxides are still by far the most popular systems among recent studies, but oxophillic 5B-6B group metals isolated on transition metal oxides, *i.e.* supported monomeric/isolated oxometallates discovered decades ago [31–33], also have to be mentioned.

This chapter covers total oxidation reactions (including CO oxidation), WGS, and selective oxidations on most types of SAC, including so-called single-atom alloys (SAA) [34]. Although some reforming reactions such as methane steam reforming include an oxidation step, they are not addressed in this chapter, and the reader is referred to the dedicated Chapter 11. While gas-phase oxidations have been mostly carried out on oxide-supported SAC, liquid-phase oxidations have often relied on carbon-hosted SAC. In the following, we have chosen to mostly focus on experimental investigations providing clear evidence of metal site isolation, though in some cases "pseudo SAC" [35] in the form of loosely packed clusters, rafts, multimers, or other atomically dispersed metal species (present by choice, lack of control, or through restructuring [26]) may be considered as well.

2. Oxide-supported single-atom catalysts

In their pioneering article, Zhang and coworkers reported on an investigation of Pt/FeO_x SAC for CO oxidation [25]. Though the current SAC literature is dominated by carbon-based materials (especially for electrocatalytic applications), most of the works on SAC in the early 2010s and before, used transition metal oxides as the support, and this field is still very active [36,37]. In addition to recent SAC studies on late transition metals, it has been known for decades that various selective (mild) oxidation reactions are well catalyzed by oxide-supported molecular structures consisting of early transition metals coordinated to oxygen atoms, *i.e.* oxometallates. At low coverage of active early transition metals, the corresponding solids can be considered as SAC.

Due to their chemical and mechanical properties, metal oxides are the most widely employed supports in heterogeneous catalysis. The first role of the oxide support is to efficiently stabilize metal NP through iono-covalent interactions. The strength of metal-support interaction strongly depends on the nature of both entities, and typically increases with the metal oxophilicity and oxide support reducibility, including in the case of SAC [38–41]. Transition metal oxides are particularly important for oxidation reactions, where they can play an active role owing to their acid-base properties, the direct involvement of lattice oxygen and oxygen vacancies (O_v - Mars-van Krevelen, MvK, mechanism [42]), and the surface diffusion of reactive intermediates between active metal species (spillover).

The first and main part of this section is devoted to CO oxidation, as this reaction is by far the most investigated for SAC, mostly based on noble metal active centers. The subsequent sections concern SAC applications to preferential CO oxidation (PROX) in the presence of dihydrogen, WGS, total oxidations, and selective oxidations. A few examples of atomically dispersed metal active sites in zeolites are also included in this section.

2.1. CO oxidation

Carbon monoxide oxidation ($2\ CO + O_2 \rightarrow 2\ CO_2$) catalyzed by platinum-group metals (PGM) has been deeply investigated and used as a model catalytic reaction for a century [43]. CO oxidation has become especially important with the development of automotive catalytic converters in the 1970s to meet emission control regulations [44]. Nowadays, three-way catalysts on gasoline-powered vehicles typically consist of Pt, Pd, or Rh NP, and sometimes SAs, dispersed on a porous oxide for converting CO as well as unburnt hydrocarbons and nitrogen oxides [44–46]. Because three-way catalysts represent the largest commercial use of these precious metals, significant research efforts have focused on SAC for exhaust pollution mitigation, including CO oxidation [47–50]. In the following sections, we highlight results from the recent literature associated with CO oxidation over late transition metal atoms anchored on non-reducible (including Al_2O_3) and reducible (including FeO_x, TiO_2, and CeO_2) oxides.

2.1.1. PGM on alumina

As early as in the 1950s, Yang and Garland ascribed CO-FTIR features at 2027 and 2095 cm^{-1} to Rh_{SA} dicarbonyls adsorbed on alumina and investigated their reaction with O_2, H_2 and H_2O, making their 2 wt% Rh/Al_2O_3 sample one of the first reported examples of SAC [15]. More recently, Yates and coworkers confirmed the previous IR assignment for $Rh^I(CO)_2$ on alumina [51], and could photochemically convert these species, in the presence of O_2, to $Rh^I(CO)(O)_x$ species and CO_2 at sub-ambient temperature [16]. From *ab initio* molecular dynamics simulations – based on density functional theory, DFT – applied to CO oxidation on Rh/γ-Al_2O_3(110), Ghosh and Nair proposed a two-step (thermal) reaction scheme where O_2 dissociates on the Rh atom, CO reacts with chemisorbed O, producing CO_2 and leaving an O atom coordinated to Rh and Al atoms [52]. Then, a second CO molecule enters the cycle, followed by a second O_2 molecule, leading to $Rh(O)_2$ and CO_2, which terminates the cycle

(**Figure 1a**, path A). The breaking of the Rh-C bond constitutes the rate-determining step. An alternative pathway (path B) was also proposed. Notably, the alumina support is continuously involved in the reaction path, in order to accommodate an O atom also bonded to the Rh atom.

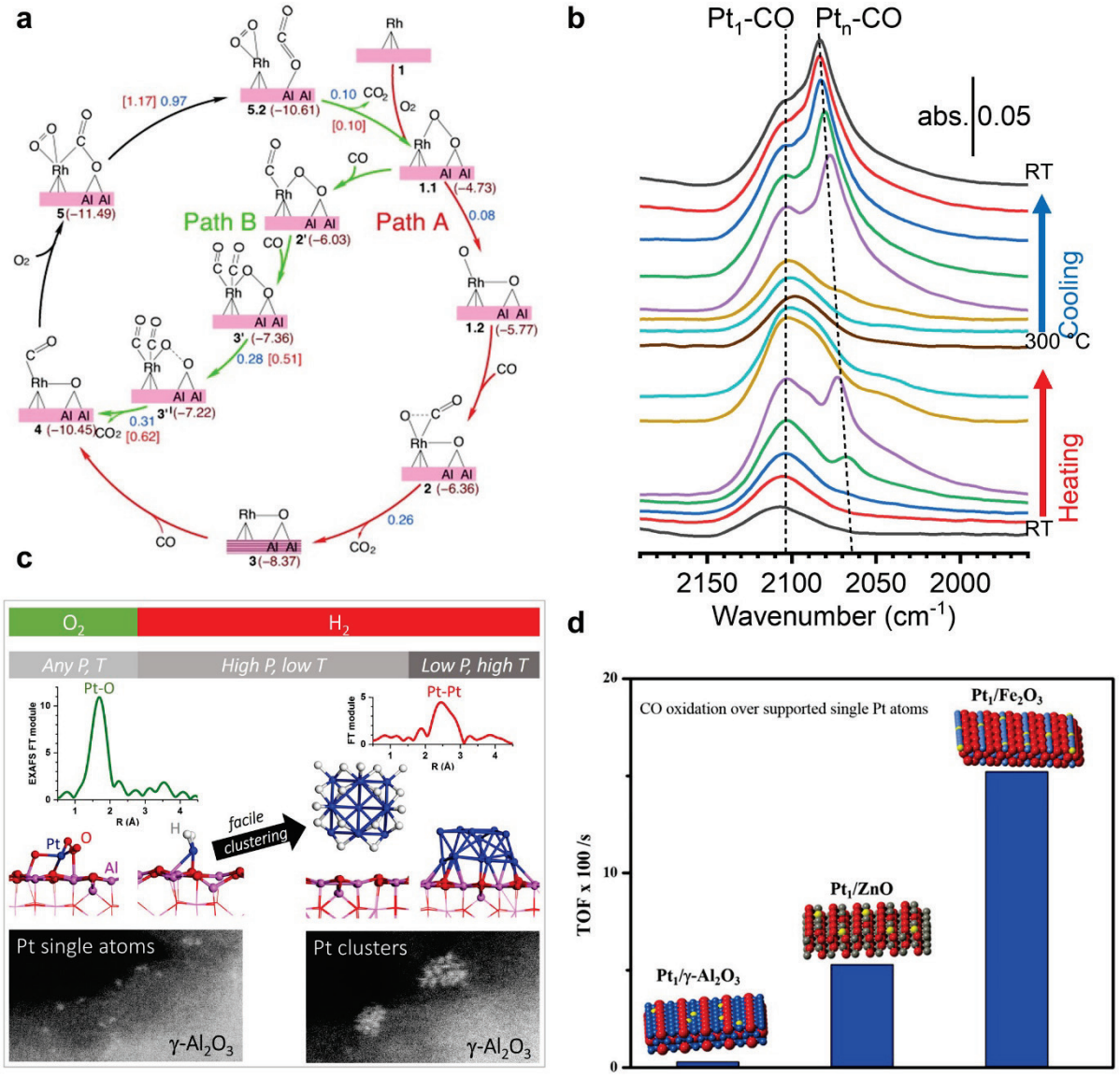

Figure 1. a) Proposed reaction schemes for CO oxidation on $Rh_{SA}/\gamma\text{-}Al_2O_3$ based on DFT calculations. Reproduced with permission from [52], Copyright 2013 Wiley-VCH. **b)** DRIFTS spectra in the C-O stretching region for an atomically-dispersed 0.3 wt% $Pt/\gamma\text{-}Al_2O_3$ catalyst under $CO\text{-}O_2$ mixture (2:2 vol%). Adapted with permission from [53], Copyright 2019 ACS. **c)** Influence of the reactive

atmosphere (O_2 vs H_2) on Pt nuclearity and atom coordination. From top to bottom: EXAFS, DFT models, and environmental STEM images. Reproduced with permission from [54], Copyright 2019 RSC. **d)** Comparison of the CO oxidation activities of single Pt atoms supported on γ-Al_2O_3, ZnO and Fe_2O_3. Reproduced with permission from [55], Copyright 2017 ACS.

In contrast, from their experimental and theoretical investigation of CO oxidation over a 0.18 wt% Pt/θ-Al_2O_3 SAC, Moses-DeBusk *et al*. introduced a reaction scheme without direct involvement of the support [28]. O_2, then CO, would adsorb on the Pt_{SA}, forming a bidentate Pt carbonate, followed by the release of a CO_2 molecule. In a second step, CO adsorbs on Pt(O), which leads to the production of CO_2 and the regeneration of the Pt_{SA}. However, the first CO_2 formation step – from $Pt(CO_3)$ – was found highly endergonic (2.22 eV), suggesting that the SAC would be covered with carbonates at room temperature. The existence of the $Pt(CO_3)$ species was supported by a diffuse reflectance infrared spectroscopy (DRIFTS) study of CO adsorption, showing an absorption feature at 1659 cm^{-1}.

Newton *et al.* investigated an industrial 5 wt% Pt/γ-Al_2O_3 catalyst by DRIFTS and X-ray absorption spectroscopy (XAS) combined with mass spectrometry under alternate CO/O_2 pulses [56,57]. The authors suggested that periodic CO_2 formation at room temperature is mediated by Pt carbonates (IR feature at ~1690 cm^{-1}) associated to single Pt cations coexisting with Pt_{NP}. Under CO, CO_2 would be released through the $Pt(CO_3) \rightarrow Pt(O) + CO_2$ reaction, as in the work by Moses-DeBusk *et al*. However, under O_2, Pt(O) would convert to $Pt(O)_2$ thanks to the neighboring presence of Pt_{NP} which enable O_2 dissociation, as well as CO storage. $Pt(O)_2$ is then converted back to $Pt(CO_3)$ under the next CO pulse.

Also using DRIFTS of adsorbed CO, Ding *et al*. investigated catalysts with various Pt SA/NP ratios and various supports, including HZMS-5 mesoporous zeolite, SiO_2, γ-Al_2O_3, TiO_2, and

ZrO_2 [58]. For alumina, IR bands centered at ~2100 cm^{-1} and ~2050 cm^{-1} were assigned to CO adsorbed on SA and NP, respectively. Upon replacing CO with O_2 – or H_2O for the WGS reaction – at 100 °C, only the CO/NP band vanished while the CO/SA band remained unchanged. This indicates that, for both reactions and all oxides, only NP are active at this temperature, while Pt_{SA} would act as spectator species owing to the strong binding of CO molecules (carbonates were not mentioned).

The above report, mostly based on IR measurements at low temperature and under model conditions, seriously questioned the CO oxidation efficiency of oxide-supported noble metal-based SAC. Using *operando* DRIFTS and XAS coupled with online mass spectrometry, Dessal *et al*. investigated CO oxidation over a 0.3 wt% Pt/γ-Al_2O_3 (157 m^2/g) SAC prepared by a conventional impregnation-calcination method [53]. Both techniques revealed a gradual Pt aggregation-activation process during heating/cooling cycles. **Figure 1b** shows a series of DRIFTS spectra recorded under CO-O_2 mixture during a temperature cycle, showing the appearance of a C-O stretching band (~2070 cm^{-1}) corresponding to *in situ* formed nanometric Pt clusters at 100 °C, which vanishes at higher temperatures due to full CO conversion (as monitored by mass spectrometry). Comparatively, CO species vibrating at ~2100 cm^{-1}, assigned to CO on Pt_{SA}, were strongly adsorbed and appeared much less reactive, in agreement with the work by Ding *et al* in [58]. **Figure 1c** shows the respective influences of O_2 and H_2 adsorption on Pt nuclearity, as seen from *in situ* extended X-ray absorption fine structure (EXAFS), environmental STEM, and DFT calculations [54]. While Pt-O_{ads}-Al bonds form under pure O_2 and stabilize the Pt_{SA} in place, the adsorption of H_2 – just like that of CO, even under excess O_2 – induces Pt clustering and reduction. The resulting H-covered subnanometric Pt clusters are mobile on the surface. Overall, evidence supports the conclusions that alumina-supported cationic Pt_{SA} are prone to clustering in the presence of reducing gases, and they are less active for CO oxidation than their Pt cluster or NP counterparts.

While the question of the intrinsic activity of Pt/Al_2O_3 SAC and their operation mechanism is still open, the influence of the support composition has been analyzed by Lou and Liu [55]. The authors compared γ-Al_2O_3, ZnO, and Fe_2O_3 solids loaded with Pt at ultralow content (0.03-0.04 wt%) deposited by a strong electrostatic adsorption method. The CO oxidation turnover frequency (TOF) at 140 °C ranges from 0.003 to 0.053 and 0.15 s^{-1} for Pt/γ-Al_2O_3, Pt/ZnO, and Pt/Fe_2O_3 SAC, respectively (**Figure 1d**). This suggests that the SAC activity increases with the oxide reducibility, and that the support directly influences the nature of the active sites. However, as discussed further below, the increasing reactivity of Pt SAC with increasing support reducibility does not always hold true (*e.g.* for CeO_2) because the support reducibility also controls how strongly the Pt atom coordinates to the support.

As mentioned above, the stabilization of SAC in general, and of single noble-metal atoms on irreducible oxides in particular, is a major challenge in SAC research, especially when reducing molecules such as CO and H_2 are present in the reactant feed [26,59,60]. However, strategies have been developed to address this issue for Al_2O_3 supports. For example, Zhang *et al.* succeeded in the synthesis of thermally stable 0.2 wt% Pt/Al_2O_3 SAC by anchoring the Pt atoms in the internal surface of mesoporous alumina (ca. 200 m^2/g) through a one-pot sol-gel method (self-assembly complexing of H_2PtCl_6, Al isopropoxide and P123 polymer) followed by air calcination and H_2 reduction [61]. The SAC was found active not only for CO oxidation but also for H_2-involving reactions. The Pt cations are thought to coordinate with unsaturated pentacoordinate Al^{3+} centers [62] *via* four O bridges. Another anchoring strategy relies on dopants such as La^{3+} and Ba^{2+} [63,64].

2.1.2. PGM on iron oxide

In 2011, Qiao *et al*. popularized the concept of SA catalysis through an analysis of platinum supported on iron oxide (290 m^2/g) [25]. Using a coprecipitation method with chloroplatinic

acid as the metal precursor, they prepared a SAC with 0.17 wt% Pt loading. The catalyst was characterized by STEM, XAS and *in situ* Fourier transform infrared spectroscopy of adsorbed CO (CO-FTIR). This work initiated the widespread use of aberration-corrected STEM imaging to complement traditionally used spectroscopic techniques to reveal or confirm the isolated nature of supported metal atoms, as well as their oxidation state [27]. The SAC exhibited a *ca*. twice superior TOF, both for CO oxidation at 27 °C and PROX at 27 and 80 °C, with respect to its Pt cluster-containing counterpart, which was prepared from the same method though with a much higher Pt loading (2.5 wt%). Based on DFT calculations, this result was ascribed to the cationic nature of Pt atoms, which would reduce both the CO-Pt binding strength and the reaction barriers. The authors also suggested that Pt atoms occupy the positions of surface Fe atoms and coordinate to *ca*. three O atoms. The same group later reported similar investigations of Ir/FeO_x SAC, which were found less active than the Pt/FeO_x SAC [65] as well as Ir subnanometer clusters supported on FeO_x [66].

In a recent investigation of Pt supported on amorphous Fe_2O_3 nanosheets, Chen *et al*. found an even larger superiority of the SAC compared to cluster-based catalysts for CO oxidation around 70 °C [67]. This result was ascribed to the positive role of the amorphous support structure on the presence of Pt-stabilizing defects with decreased CO adsorption energy, and the abundance of O_v prone to activate O_2. The scanning tunneling microscopy (STM) study of Parkinson and coworkers on a $Pt_{1\text{-}6}/Fe_3O_4(001)$ model catalyst (resulting from the CO-induced partial sintering of initially single Pt atoms) provides a striking atomic-scale visualization of CO-induced lattice O extraction at the perimeter of Pt clusters, which often sit at the edge of or inside monolayer holes in the oxide surface (**Figure 2a**) [68]. The corresponding formation of gaseous CO_2 and O_v constitutes the first step of the MvK mechanism. The second step involves the replenishment of O_v from gas-phase O_2 (absent in the case of **Figure 2a**). Islands of O_v were observed to increase in size under exposure of the model catalyst to H_2, which leads to water evolution *via*

Pt-induced hydrogen spillover and OH group formation (**Figure 2b**). In contrast, exposure to O_2 leads to the filling of O_v and the creation of $Fe_3O_4(001)$ islands through oxygen spillover and reaction with bulk Fe atoms (**Figure 2c**).

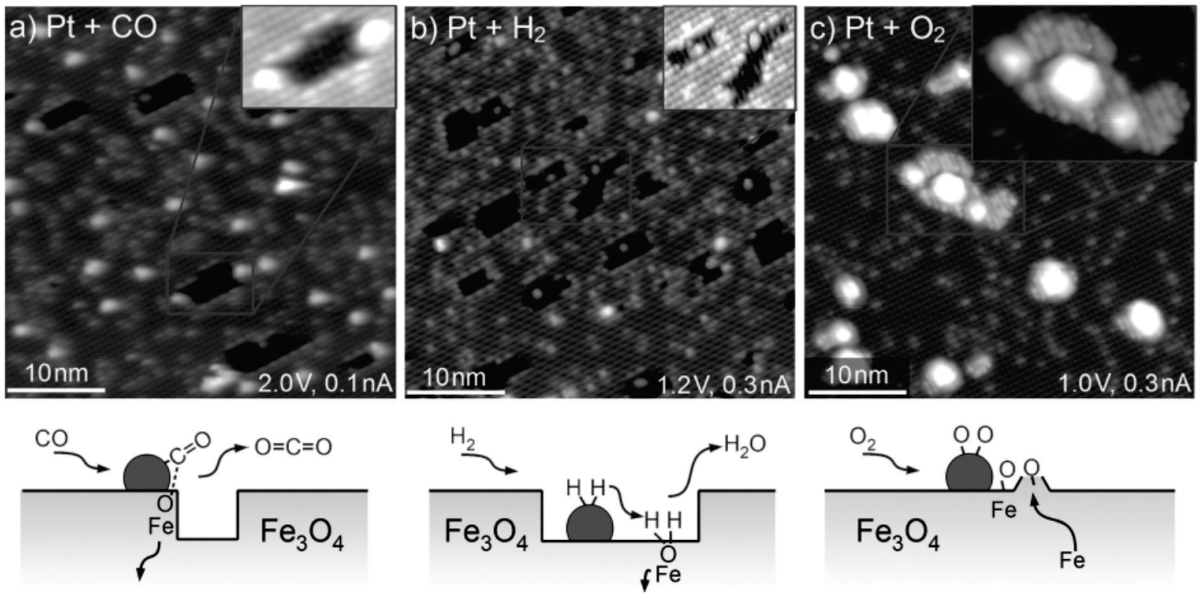

Figure 2. STM images acquired following exposure of the $Pt/Fe_3O_4(001)$ model catalyst to 1×10^{-7} mbar of CO **(a)**, H_2 **(b)**, or O_2 **(c)** at 277 °C, and illustration of the corresponding surface processes. Adapted with permission from [68], Copyright 2015 Wiley-VCH.

In a recent study of the model $Rh/Fe_3O_4(001)$ SAC using STM, X-ray photoelectron spectroscopy (XPS) and temperature-programmed desorption (TPD), the same group identified an O_2-induced Rh oxidation/clustering process, whereas CO strongly adsorbs and stabilizes Rh adatom isolation [69]. Under these high-vacuum conditions, while RhO_x clusters catalyze CO oxidation at sub-ambient temperature through the classical Langmuir-Hinshelwood (LH) mechanism, Rh carbonyls can only catalyze the reaction through the MvK mechanism at higher temperature.

The existing works on Pt and Rh SAC on FeO_x supports are consistent in proposing MvK as the primary reaction mechanism, although the reactivity of the SAC seems to be controlled by the nature of the FeO_x support (phase and surface structure).

2.1.3. Noble metals on titania

TiO_2 has long served as a model oxide that imparts distinct catalytic chemistry onto supported metal active sites. For example, TiO_2 is the classic support that enables strong metal-support interactions with Pt-group metals and one that provides size-dependent reactivity to supported Au particles [70,71]. TiO_2 has similarly served as a model system for understanding the structure, dynamic behavior, and reactivity of SAC active sites. Particularly, small anatase crystallites have been demonstrated as supports that allow for the synthesis of atomically dispersed Pt species with uniform local coordination environments rivaling single-crystal oxides and zeolite supports. The uniformity of the Pt active sites enables unambiguous spectroscopic fingerprinting, structural analysis, and the development of structure-function relationships.

SAC have been synthesized using small (~5 nm diameter) anatase TiO_2 crystallites, low Pt loadings (<0.1 wt%), and principles of strong electrostatic adsorption. Aberration-corrected STEM imaging was used to demonstrate the existence of solely Pt_{SA} in these samples (**Figure 3a**) [72–74]. Probe-molecule CO-FTIR spectroscopy and TPD were used to chemically characterize the Pt active sites (**Figure 3b**). It was observed that following 250 ºC reduction of the catalyst in H_2, bound CO exhibited a vibrational wavenumber of ~2112 cm^{-1} with a full-width at half maximum lower than 10 cm^{-1}.

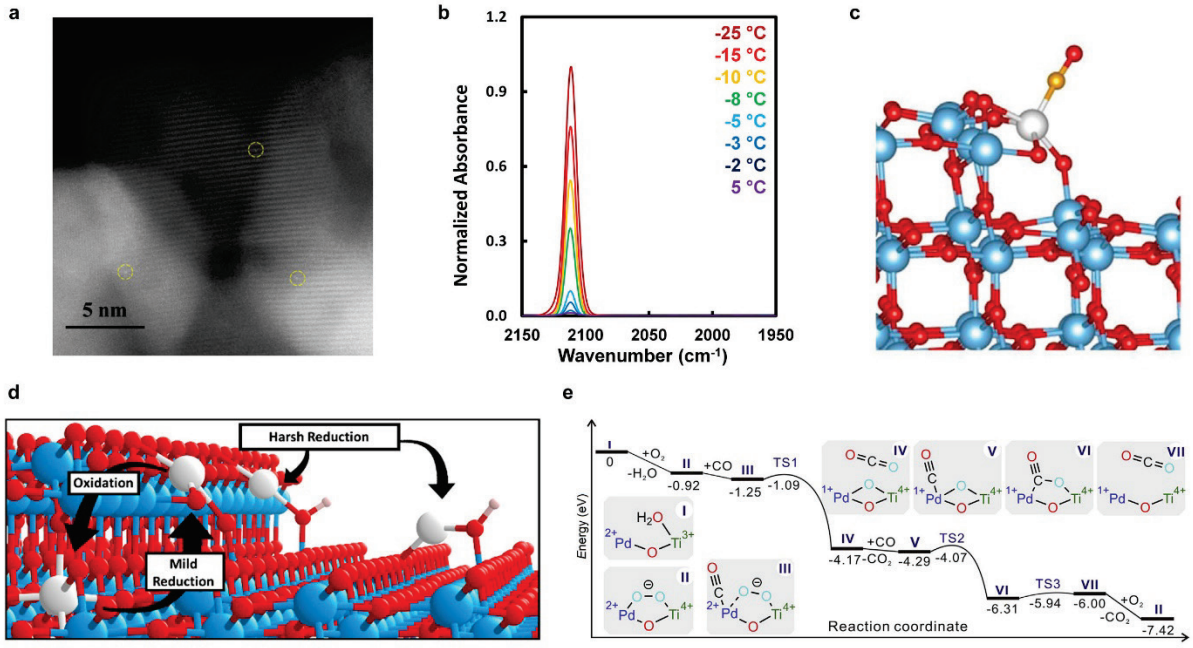

Figure 3. a) Aberration-corrected STEM image of Pt atoms (identified by yellow circles) on ca. 5 nm diameter anatase TiO_2 particles. Adapted with permission from [72], Copyright 2017 ACS. **b)** CO probe-molecule FTIR spectra of a Pt/TiO_2 SAC as a function of temperature during a TPD measurement. **c)** DFT-calculated structure of CO bound to PtO_2 adsorbed at a TiO_2(145) step edge. **b** and **c** adapted with permission from [73], Copyright 2018 Elsevier. **d)** Schematic showing the structural transformation of isolated Pt species as a function of environmental conditions. Adapted with permission from [74], Copyright 2019 Springer Nature. **e)** DFT-calculated reaction pathway for CO oxidation on a Pd/TiO_2 SAC that was supported by spectroscopic and kinetic analyses. Adapted with permission from [75], Copyright 2018 Elsevier.

This suggested that Pt existed in a +2 oxidation state with a uniform coordination environment across the support [72,76,77]. TPD measurements showed an approximate CO binding energy of 0.9 eV (~87 kJ/mol). Detailed comparisons to many different Pt coordination environments on TiO_2 (101) and (145) surfaces allowed the identification of adsorbed PtO_2 species at terrace or step edges as the most representative coordination environment of the atomically dispersed

Pt active sites (**Figure 3c**) [73]. This assignment was further substantiated through site-resolved STEM imaging and EXAFS analyses, which showed quantitative and visual correlation between the DFT-predicted structure and the experimental analysis [74]. Consistency between the chemical (oxidation state, CO adsorption energy and CO vibrational frequency) and structural (STEM imaging and EXAFS analysis) analyses from experiments and theory was only feasible because of the highly uniform Pt local coordination environment on the anatase TiO_2 support.

While the Pt active-site structure on anatase TiO_2 was well resolved after a particular pre-treatment, it has been further demonstrated that the Pt local coordination environment is adaptive to variations in temperature, oxidizing or reducing chemical species, and photochemical stimulation [74,78–82]. For example, it was inferred from a combination of microscopy, spectroscopy, and theory that Pt prefers to reside in a cation-replaced position in the TiO_2 lattice with 6-fold coordination to oxygen following oxidizing pre-treatment; an adsorbed PtO_2 state following mild reducing pre-treatment; and as a mobile PtOH species under harsher reducing conditions (**Figure 3d**) [74]. Further analysis under much harsher reducing environments has shown that the coordination environment of Pt species could involve direct coordination to H and access unique support coordination environments [80,81]. Finally, it has been shown that extended exposure to CO oxidation reaction conditions and photochemical environments can sometimes lead to the formation of Pt clusters [78,79,82]. The adaptive nature of atomically dispersed Pt on TiO_2 suggests that the reactivity of these active sites can likely be tuned by controlling the coordination environment, and also that the active-site structure may be different following pre-treatment and exposure to reactive environments. Interestingly, it has also been observed that other atomically dispersed metals, such as Cu and Rh, exhibit similar dynamic physical and electronic structures as a function of environmental conditions [83,84].

The reactivity of Pt/TiO_2 SAC have been assessed both from chemical (how strongly species bind to Pt sites) and catalytic (rates of reactions) perspectives. CO-FTIR and TPD measurements correlated to DFT calculations showed that CO binds more strongly to *ca*. 1 nm diameter metallic or oxidized Pt clusters on TiO_2, as compared to atomically dispersed Pt sites. This is particularly interesting because CO bound to Pt_{SA} and small PtO_x clusters exhibited almost identical stretching frequencies (~2110 cm^{-1}) but binding energy differences superior to 100 kJ/mol, due to the undercoordination of Pt in partially reduced PtO_x clusters. This highlights an important challenge in using CO-FTIR to characterize Pt SAC, and makes a strong point that the co-existence of Pt_{SA} and small oxidized Pt clusters on a support can be easily confused.

It has been shown under multiple reaction conditions that Pt_{SA}/TiO_2 catalysts exhibit higher CO oxidation activity on per Pt mass and per Pt site bases as compared to small Pt NP; this is consistent with what has been observed for Pt/FeO_x [72,85]. Furthermore, it has been shown that coordination environments, which resulted in close to neutral atomically dispersed Pt, exhibited stronger binding to CO and higher CO oxidation activity as compared to coordination environments where Pt existed in a +2 oxidation state [74]. However, there have also been reports claiming that Pt_{NP} on TiO_2 are actually more reactive than Pt_{SA} on TiO_2 [79]. The differences in conclusions regarding the relative activities of atomically dispersed Pt and Pt_{NP} on TiO_2 likely point to the critical role of the support structure, Pt precursor (for example H_2PtCl_6 can lead to Cl poisoning of active sites), and Pt coordination environment in controlling the catalytic performance.

The use of TiO_2 as a support for atomically dispersed metals is not limited to Pt. Reports of CO oxidation on Au/TiO_2 and Pd/TiO_2 have provided further evidence of high activity from atomically dispersed metals on TiO_2 [75,86]. For example, it was reported that Pd_{SA}/TiO_2 catalysts exhibit the highest activity for CO oxidation compared to all previous reports on Pd-based catalysts. It is clear from our review of the literature above that various groups have

measured enhanced CO oxidation activity from atomically dispersed precious metals on TiO_2 as compared to NP of the same metal. Reports countering this conclusion also exist, which highlights the challenge in studying this class of materials. Finally, it has been observed that the reactivity of atomically dispersed Pt species could be further promoted by localizing Pt at CeO_2-TiO_2 interfaces [87]. This observation again points to the critical role that local coordination plays in dictating the reactivity of atomically dispersed Pt, and suggests that supports likely participate directly in the CO oxidation reaction.

Mechanistic analysis of CO oxidation over Pt/TiO_2 and Pd/TiO_2 through DFT calculations, kinetic measurements coupled to microkinetic modeling, and spectroscopic analysis have provided a consistent picture [74,75,85]. Generally, it has been proposed that the reaction proceeds *via* an MvK mechanism, with formation of an O_v at the Pt(Pd)-TiO_2 interface, followed by O_2 adsorption and dissociation, and then CO adsorption and oxidation (**Figure 3e**). Consistency in each of the proposed mechanisms is found in the observation of less CO poisoning on single metal atoms as compared to metal clusters of the same composition. This derives from the cationic oxidation state and strong support coordination of the metal SA. However, details regarding rate-determining steps, reaction orders, and apparent barriers are specific to each case where small differences in support (for example anatase versus rutile, or defect concentration) and metal (coordination environment, site uniformity) are critical for dictating reactivity.

2.1.4. Late transition metals on ceria

Cerium oxide (CeO_2) has been extensively investigated for many reactions both as a catalyst and a support [88–91]. The distinct catalytic performances of CeO_2 derive from unique physical properties, including high reducibility while remaining in its fluorite structure, easy electron transfer between Ce^{4+} and Ce^{3+} cations, high mobility of surface oxygen species, and high

oxygen storage capacity [88–90,92,93]. Furthermore, defects such as O_v and Ce^{3+} can be stabilized in nanocrystallites contained in ceria supports, leading to sub-stoichiometric oxides [94,95]. CeO_2 also contains at its surface both acid and basic sites in close proximity [89]. In particular, a high proportion of strong basic sites can be present, leading to easy carbonation, which can influence the catalytic reaction [96]. The redox properties of ceria have made it an ideal PGM support for automotive catalytic converters, which is currently the main application of this material; in particular, Pt, Pd and Rh NP supported on CeO_2 exhibit excellent CO oxidation performances [97,98].

M/CeO_2 SAC with M = Pt, Rh, Cu, and Au have been prepared by various methods including classical incipient wetness impregnation [99], atomic layer deposition [100], and gas phase atom trapping where volatile MO_x species adsorb and are stabilized on some support surfaces [101]. For example, atomically dispersed metals have been shown to be stabilized on certain facets of CeO_2 by an a oxidizing treatment at 800 °C [99–102]. In the case of Pd_{SA}/CeO_2, high-temperature atom trapping by calcination at 800 °C increased the amount of O_v, resulting in decreased Pd−O (lattice oxygen from CeO_2) coordination in square planar Pd_1O_4 [103]. Defect sites can serve to stabilize noble metal catalysts with atomic dispersion by adsorption of ascorbic acid to generate Ce^{3+} cations [104], or by doping with Ga^{3+} or Zr^{4+} cations [105,106]. Similarly, a CeO_2/Al_2O_3 support containing smaller CeO_2 particles and more surface defects led to more atomically dispersed Pt and abundant Pt-O-Ce structures [107]. In fact, the defect-induced trapping of metal cations such as Au^+ or Au^{3+} [108], or mobile metal oxide species such as PtO_2 [109], have been proposed to lead to the exclusive formation of atomically dispersed metals.

However, the exact location and coordination of Pt_{SA}, as well as the potential existence of small oxidized PtO_x clusters in samples previously reported as SAC, is still debated. The challenge with providing conclusive evidence of Pt site isolation on CeO_2 stems from the heavy mass of

Ce, which minimizes contrast with Pt in STEM imaging, and the fact that XAS is a sample-averaged technique. Early on it was proposed that Pt_{SA} prefer to sit in 4-fold coordinated symmetric Pt-O_4 CeO_2 micro-environments, and be rendered inactive for molecular adsorption by the formation of a highly stable Pt d^8 structure [110]. However, various experimental reports have claimed to identify Pt SA on CeO_2 through CO-FTIR based on a stretching band at 2095 cm^{-1}, which is stable at high temperature [101,109,111,112].

The location of these Pt atoms on CeO_2 has been claimed to range from {111} ceria steps or {111}, {110} or {100} ceria facets, to surface or bulk Ce substitutes forming $Ce_{1-x}Pt_xO_{2-y}$ solid solutions (Ref. [113] and references therein). In an attempt to clarify the structure of Pt single sites determined by DFT calculations, experimental EXAFS data were fitted with theoretical ones by Maurer *et al*. [113]. As shown in **Figure 4a-l**, the fit substantially improves for several exposed facets, going from adsorbed to surface-substituted Pt species. The agreement is quite good within the radial distance range 1.1-3.4 Å for models with Pt^{2+} substituted at {110} facets, which corresponds to four-fold hollow sites. Within the best-fit model, adsorbed CO is predicted to have a stretching frequency of ~2095 cm^{-1}, consistent with experimental measurements. However, it has been noted that using CO vibrational frequency to correlate DFT-calculated structures and experimental measurements can lead to misassignment, and that additionally comparing the CO adsorption energy is critical for substantiating a DFT-based structural assignment [73,114]. Based on this issue and detailed microscopy and spectroscopy analysis, Resasco *et al*. proposed that the 2095 cm^{-1} signature found in Pt/CeO_2 catalysts stems from the existence of CO adsorbing to a sub-population of small Pt_xO_y clusters that are challenging to detect by STEM or EXAFS [115]. Thus, it seems that there is still a disagreement in literature on spectroscopic assignments associated with atomically dispersed Pt species on CeO_2, which highlights the interesting and challenging nature of studying SAC.

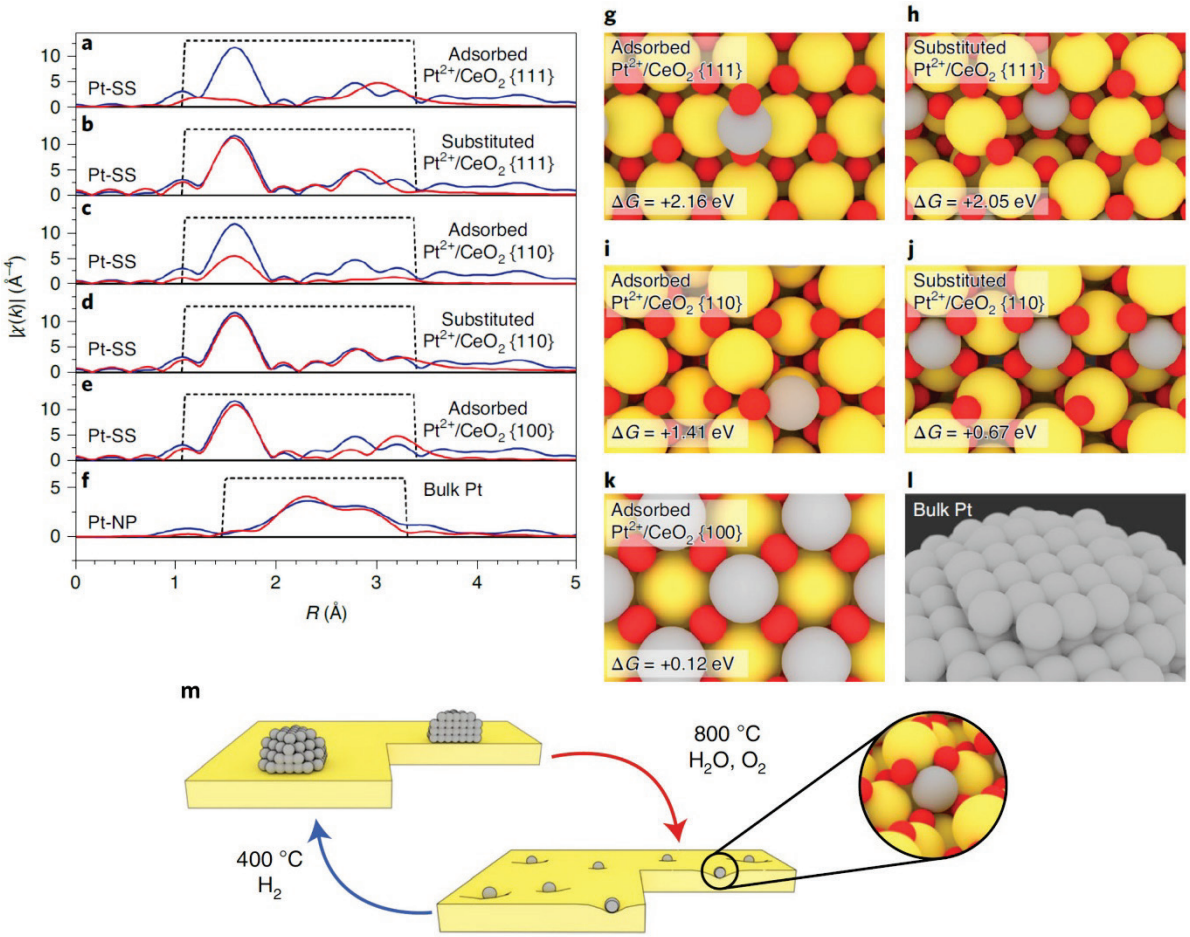

Figure 4. EXAFS analysis of a Pt/CeO_2 SAC. **a–f)** Fourier transform k^3-weighted EXAFS data for Pt single sites and Pt NP recorded at the Pt L_3 edge. The experimental data (blue) were fitted (red) in the range 1.1–3.4 Å (dashed box) using five possible locations of Pt^{2+}. Bulk Pt was used to fit Pt NP. **g–l)** The corresponding structures (grey, Pt; yellow, Ce; red, O), as determined by DFT calculations, showing the free-energy values. **m)** Illustration of Pt nanoparticle redispersion and Pt-induced restructuring of the CeO_2 support at high temperatures under oxidizing conditions as well as particle formation from the atomically dispersed state under reducing conditions. Adapted with permission from [113], Copyright 2020 Springer Nature.

The catalytic properties of M_{SA}/CeO_2 catalysts depend on the oxidation state of the metal. For instance, oxidized Pt_{SA} presented poorer activity than Pt_{NP}, whereas metallic Pt_{SA} showed higher activity for the oxidation of CO, NO and CH_4, which is consistent with observations for Pt/TiO_2 [116]. However, the common assignment of a fixed oxidation state of metal atoms in SAC is

oversimplified. Daelman *et al*. identified several well-defined charge states that are dynamically interconnected by combining DFT calculations and first-principle molecular dynamics on Pt_{SA} adsorbed on the CeO_2(100) surface [117]. A similar analysis was published simultaneously by Alexopoulos *et al*. for Pd/Al_2O_3, which also demonstrated the dynamic charge state of SAC during CO oxidation [118].

The dynamic behavior suggests that *in situ* measurements of SA oxidation states probe the state of the most abundant species in the catalytic cycle. The study of electron transfer between the metal and CeO_2 determined by the relative positions of the Ce 4f levels with respect to those of the noble metal is crucial to understand the nature of the active site and the associated reaction mechanism. Pt-O-Ce bond formation is favored by the presence of defects such as O_v associated with Ce^{3+} cations [109,119,120], and their proportion was related to the distortion degree of the interface. In this regard, Pt_{SA}/CeO_2 sites were constructed at continuously-twisted surfaces in a monolith by directly growing porous CeO_2 single crystals and confining Pt in the lattice [121]. It was shown that these sites not only contribute to the chemisorption of CO but also effectively activate the lattice oxygen linked to Pt ions for CO oxidation. In fact, the distortion of Pt-O-Ce bonds, which is energetically favorable through strong metal-support interaction, balances the Fermi energy and the charge density between the Pt species and the CeO_2 support, leading to variations in the valence state and the electronic structure of Pt_{SA}/CeO_2 [120]. Note that a correlation between the strength of the Pt-oxide/oxide-support interaction and the electron density of oxygen in oxide supports was reported [122]. The latter, as determined from the binding energy of the O 1s electron, was found maximal for CeZrY mixed oxide and CeO_2, and minimal for Al_2O_3 and SiO_2.

Furthermore, the local coordination environment of SA determines their catalytic activity. For example, a hydrothermal treatment was suggested by Nie *et al*. to create a new type of thermally stable $O_{lattice}H$ active site in the vicinity of Pt^{2+}, leading to enhanced catalytic activity for CO

oxidation [111]. Besides, the addition of phosphorus (an electron acceptor) into CeO_2 was reported by Ma *et al*. to considerably decrease the electron density of Pt atoms [123]. Their higher valence state gave rise to an activity enhancement by up to 10 times in the hydrogenation of styrene, cyclohexene, phenylacetylene, and nitrobenzene. It was also shown that phosphorus favors reactant adsorption strength and hydrogen spillover, both playing an important role in this enhancement.

The catalytic performances of SAC depend on the considered reaction, and this is particularly true when they are supported on CeO_2. For instance, Au_{SA}/CeO_2 was found much more active for CO oxidation than its NP counterpart, but showed poor activity for H_2 oxidation [124]. This unique feature would be beneficial to the PROX of CO in H_2-rich gas stream (Section 2.2). CO oxidation on Pt_{SA}/CeO_2 [125] and Rh_{SA}/CeO_2 [126] was found to follow the MvK mechanism: adsorbed CO molecules react with O species to form CO_2 and O_v, which are then replenished by adsorption of O_2. On the Rh/CeO_2 SAC, the measured CO and O_2 reaction orders were 0.2 and -0.03, respectively, i.e. totally different from those obtained for the nanocatalyst counterpart (-1 and 1, respectively) that favors an LH mechanism [126]. CO oxidation on Pt/CeO_2 [112] and Au/CeO_2 [127] SAC is promoted by the presence of H_2O. For Pt_{SA}/CeO_2, CO was proposed to easily react with the hydroxyl from dissociated water to yield a carboxyl intermediate, which subsequently dehydrogenates with the help of a lattice hydroxyl to generate CO_2 and water (water-mediated mechanism) [112]. For Au_{SA}/CeO_2, the promoting effect was attributed to the local atomic and electronic structure of SAC, that facilitates an efficient reaction channel of CO with OH [127]. CO oxidation on NP periphery sites would be much less promoted by the presence of H_2O.

Controversies on the intrinsic activity of M_{SA}/CeO_2 catalysts can be found in the literature [110,111,113,128–131]. Beyond discrepancies due to the preparation method and reaction conditions, the use of *in situ* techniques is crucial to compare the performances of SAC with

those of cluster or NP catalysts [26,113,132]. It is especially true considering the dynamic structural behavior of metal/ceria catalysts, showing *e.g.* the formation of clusters or NP from SA under reducing conditions and redispersion under oxidizing conditions (**Figure 4m**), even at low temperature (< 300 °C) [133–135]. Recently, the onset of CO oxidation was found connected to the migration of Pt_{SA} from four-fold hollow sites of ceria, forming few-atom clusters [113]. This suggests that the latter are the active sites or that the dynamics of Pt_{SA}/CeO_2 contributes to CO oxidation.

2.1.5. Other catalysts

A number of other oxides have been employed as SA supports. In 2001, Abbet and coworkers reported an investigation of Pd atoms anchored to MgO(100) surface O_v (F-centers) using temperature-programmed reaction of O_2 with preadsorbed CO at -183 °C, IR spectroscopy, and DFT calculations [20]. Low-temperature (-13 °C) and high-temperature (227 °C) reaction routes were identified, with $Pd(CO)_2O_2$ and $PdCO_3CO$ found as precursors, respectively. However, the process leads to the filling of the O_v, and consequently to the migration and clustering of CO-carrying Pd atoms, as observed for Pt/Al_2O_3 [53]. Recently, Sarma *et al.* systematically investigated CO oxidation over M/MgO SAC (M = Ru, Rh, Pd, Ir, Pt) using XAS, FTIR, and DFT [136]. The metal cations were shown to occupy octahedral positions of the MgO lattice under step edges. O_2-lean $CO+O_2$ conditions lead to the partial deconfinement of the metal atoms and the formation of bidentate metal carbonate species, which would constitute the reactive intermediates. Also similar to the results obtained for alumina, the involvement of the (irreducible) MgO support was found limited, and the SAC activities were found lower than those of the supported cluster counterparts. Though Pt leads to the lowest apparent activation energy, the latter was found in the range of 96 ± 19 kJ/mol for the whole set of metals (see also Section 2.1.6 below).

Copper oxides have been used as SA supports in several studies. Though Zhou *et al*. detected no CO oxidation activity for SA in a model Pt/CuO/Cu(110) catalyst due to the weakness of CO adsorption [137], Therrien *et al*. reported that the reaction proceeds at low temperatures on a $Pt/Cu_2O/Cu(111)$ SAC [138]. In the latter case, from STM, TPD, IR, XPS, and DFT, the reaction was shown to involve lattice O atoms and neighboring charge-neutral Pt_{SA} through a MvK mechanism. CO oxidation was also shown to proceed through this mechanism over a model Au/CuO/Cu(110) SAC, in which Au_{SA} are negatively charged [139]. In a recent study by Wang *et al*., Fe_1O_3 motifs were grown on a $Cu_2O(100)$ single crystal by atomic layer deposition and characterized by near-ambient-pressure XPS, STM, and DFT [140]. The densely distributed but isolated Fe centers, with an oxidation state close to +3, were found active for CO oxidation at 200 °C. Whether Pt or Fe, the single metal atoms were shown to diffuse into the Cu_2O subsurface under reaction conditions, leading to deactivation of the model catalyst [138,140]. As pointed out by Kropp *et al*. from DFT calculations in the cases of Pt and Pd SAC supported on MeO(001) (Me = Fe, Mg, Mn, Ni), catalyst deactivation may also be caused by metal sintering due to the O_2-induced healing of the O_v that stabilize the single metal atoms (in a negatively charged state) [141].

Various other oxides, accompanied with specific synthesis strategies, have been employed as supports for CO oxidation-active SAC, *e.g*. Ir on $MgAl_2O_4$ spinel [142], Au [143] and Pd [144] on cobalt oxides, Pd on $(CeZrHfTiLa)O_x$ high-entropy fluorite oxides [145], and Pt on $Cr_{1.3}Fe_{0.7}O_3$ [146]. These studies point out the importance of surface O_v and/or structural defects such as steps for the SAC stabilization. Remarkably, a 0.067 wt% Au_{SA}/Co_3O_4 catalyst exhibited a high activity (TOF = 3.1 s^{-1}) at -75 °C, which was ascribed from DFT calculations and isotopic experiments to a predominant LH pathway over an active site composed of a Au_{SA} and neighboring Co and O/O_{vac} species [143].

Using FTIR, *operando* XAS, kinetic measurements, and DFT calculations to investigate a model Ir/$MgAl_2O_4$ SAC with an ultralow metal loading (0.0025 wt%), Lu *et al.* have proposed an original CO oxidation mechanism involving Ir(CO) species as the active supported complex and Ir(CO)(O) as the most stable intermediate [142]. The latter would be the SAC resting state involved in the rate-determining step following an Eley-Rideal mechanism: Ir(CO)(O) + CO $\rightarrow$ Ir(CO) + CO_2. Thus, CO would act as a ligand rather than a poison to (cationic) Ir atoms. Notably, the SAC exhibited reaction orders toward CO and O_2 different from those of supported Ir_{NP}, corresponding to different reaction mechanisms. This makes possible the quantification of surface site fractions in catalysts containing both SA and NP [147].

2.1.6. Discussion

A few ideas emerge from the above review of the literature: controversies regarding the characterization, local coordination environment, reactivity, and catalytic mechanisms of oxide-supported late-transition-metal atoms in CO oxidation catalysts are prevalent in literature.

The first issue is the characterization of SAC with the aims of substantiating the complete dispersion of metals as site-isolated atoms (ions) and identifying the primary local coordination of the metal species. Aberration-corrected STEM imaging executed through a combination of large-area and local measurements can effectively demonstrate the primary existence of atomically dispersed metals. However, this becomes challenging when the support oxide contains cations that have similar or high atomic number as compared to the metal atoms (*e.g.* Pt and Ce, or Rh and Ce). In these cases, additional characterization is required to assess the primary metal structure. The most common tools are XAS and CO-FTIR. Again, results from these characterization techniques can be challenging to interpret. For example, single cationic Pt atoms on an oxide support can show similar XAS and CO-FTIR spectra as compared to small

non-uniform PtO_x clusters on the same support [72,115]. Thus, it has become apparent that chemical probes – for example reducibility, measurements of the adsorption energy of a probe molecule, or reactivity of a probe reaction such as simple hydrogenation chemistry – may be best suited to analyze the relative dispersion of metals across a sample [73,115,148]. Once the latter is assessed, the uniformity of the local coordination environment should then be considered prior to assigning a dominant local coordination environment [76].

While apparent discrepancies exist in the characterization of SAC, a few common themes have emerged. First, for reducible supports, single late-transition-metal atoms tend to adopt cation-replaced position in the oxide lattice following oxidative treatments [25,74,83,84,110,117]. Exposure to reducing environments results in reduction of the oxidation state of the metal atom (ion) and likely a reduction in the M-O coordination number. Finally, harsher reduction results in the production of mobile atomically dispersed species in close to neutral states, which serve as the precursors for cluster formation. Non-reducible oxide supports such as Al_2O_3 [53,54] and MgO [136], which have softer interaction with metal atoms as compared to reducible oxides, maximize reduction and clustering phenomena in the presence of CO or H_2.

The second common theme, in the case of reducible oxide supports, is that Pt SAC tend to exhibit lower CO adsorption energies as compared to metallic Pt clusters. This stems from the cationic oxidation state of Pt in SAC, and the strong coordination to the support. A result of the decreased CO binding energy on Pt SAC is the reduced CO coverage on the Pt active site during CO oxidation [72].

Finally, as previously mentioned, two main types of CO oxidation pathways have been proposed on oxide-supported SAC, the MvK and the LH mechanisms [44,48]. The former is favored on reducible oxides, while the latter necessarily involves carbonate-like species, as illustrated in **Figure 5a**. According to the recent literature analysis by Beniya and Higashi of CO oxidation over PGM and Au catalysts supported on various oxides, Pt SAC are overall more

efficient than Pt cluster catalysts above *ca*. 100 °C, while supported Au_{NP} are superiors to SAC at low temperature [44]. However, as previously discussed in the chapter, this issue is still strongly debated, especially for the Pt/CeO_2 and Pt/Al_2O_3 systems in relation to their actual active site, owing to the dynamic evolution of the Pt atom nuclearity and oxidation state under reaction conditions.

Few experimental attempts have been made to compare the effect of the metal or the support identity on the SAC performance. Comparing PGM atomically dispersed on MgO for CO oxidation, Sarma *et al*. recently reported that Ru, Pd, and Pt are more active than Rh and Ir, and that metallic clusters are overall more active than the single cations (**Figure 5b**) [136]. Computational studies can help in the design of SAC and rationalize their *modus operandi*. Still in the case of the MgO support, using DFT calculations and microkinetic modeling, Xu *et al*. predicted from Brønsted–Evans–Polanyi relationships that Ag and Cu SAC should perform better than Ni, Pd, and Pt SAC for CO oxidation (**Figure 5c**) [149]. The LH mechanism was found to be more favorable than the MvK and Eley-Rideal pathways. Such an example can motivate future research toward the design of SAC based on non-conventional metals.

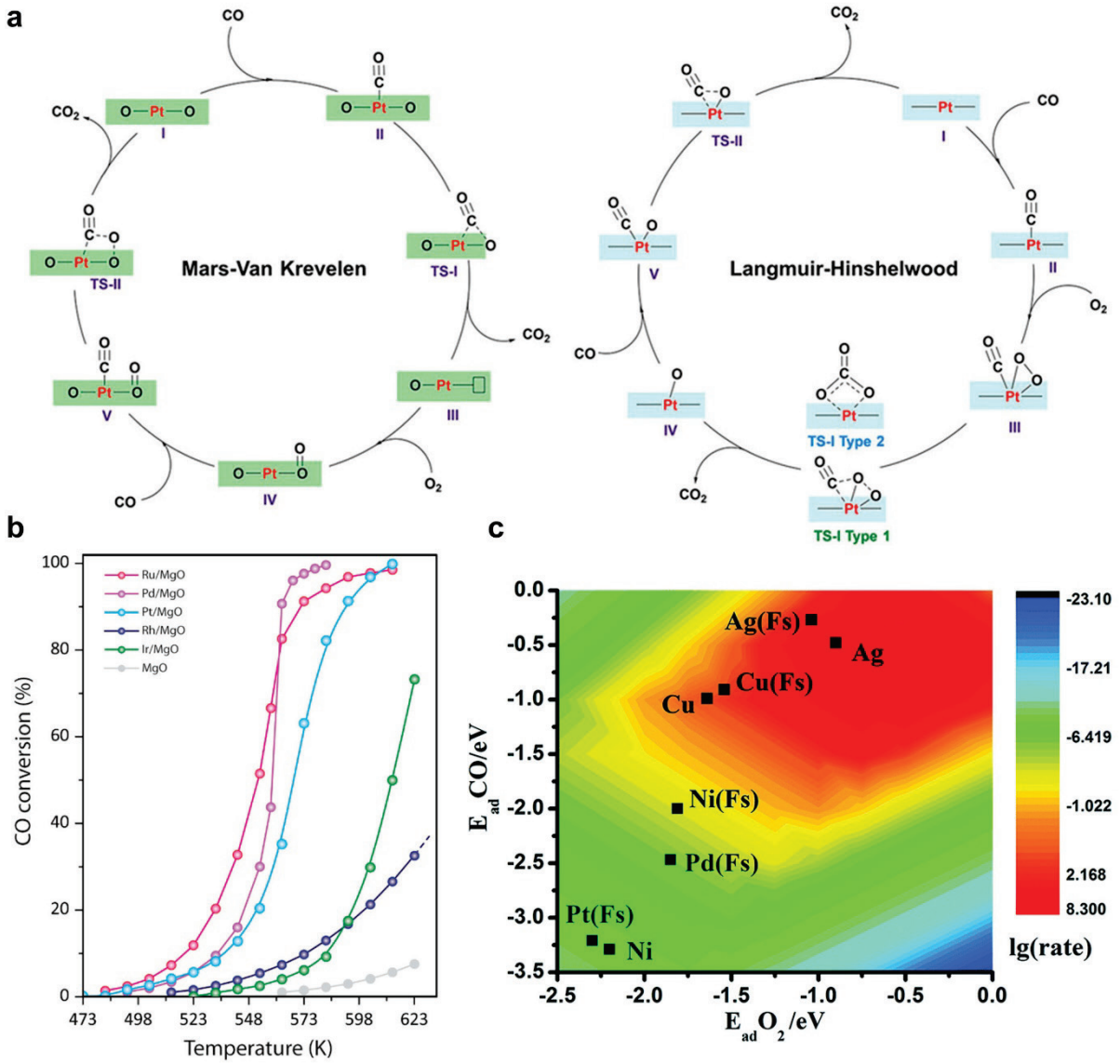

Figure 5. a) Typical reaction pathways of Pt SAC via the MvK or the LH mechanism. Adapted with permission from [48], Copyright 2020 Wiley-VCH. **b)** Evolution of CO conversion with the reaction temperature for M/MgO SAC (0.1 M_{at} nm^{-2} metal content, 1 bar, $CO:O_2$=1:20 vol%). Adapted with permission from [136], Copyright 2020 ACS. **c)** Contour plot of the Sabatier activity with respect to the CO and O_2 adsorption energies on different SAC under typical experimental conditions for low-temperature CO oxidation (T = 0 °C, P_{O2} = 0.21 bar, P_{CO} = 0.01 bar). (Fs) represents M/Fs-defect MgO. Reproduced with permission from [149], Copyright 2017 RSC.

2.2. Preferential CO oxidation in hydrogen (PROX)

Preferential CO oxidation is useful for removal of CO impurities present in hydrogen produced from hydrocarbon reforming. Such a pure hydrogen is then able to feed proton-exchange-membrane fuel cells [97]. Like for conventional CO oxidation, noble metals (especially Pt and Au) supported on reducible oxides are the most efficient catalysts for this reaction, *i.e.* they exhibit high activity and selectivity at low temperature (< 100 °C). The extension of this knowledge to SAC is challenging owing to the highly reducing hydrogen-rich atmosphere, potentially favoring metal atom clustering [54]. This may explain the scarcity of studies related to PROX on SAC.

Zhang and coworkers reported the PROX performances (reactant mixture $CO:O_2:H_2$ = 1:1:40 vol%) of Pt and Ir SA supported on iron oxide. The Ir_{SA}/FeO_x catalyst was found much less efficient than both the Pt/FeO_x SAC [65] (consistently with nanocatalysts [97]) and an Ir/FeO_x catalyst based on subnanometric Ir clusters [66]. In contrast, the Pt_{SA}/FeO_x catalyst was reported to be more active than its cluster-based counterpart [25]. The same group also investigated the PROX reaction over 0.05 wt% and 0.3 wt% Au_{SA}/CeO_2 prepared by a simple adsorption method [150]. The catalyst was found to be stable, highly active and fully selective at 70-120 °C. The high performance at relatively high temperature was ascribed to inhibited H_2 dissociation on SAC, which would disfavor the unselective route. Gan *et al*. recently reported a dry ball milling method able to produce, from acetate precursors, kilogram-scale 0.1 wt% Au_{SA}/CeO_2 for PROX [151].

Notably, several types of highly dispersed catalysts containing hydroxide species were reported to exhibit excellent PROX performances. Zhang and coworkers prepared subnanometric-cluster $Ir/Fe(OH)_x$ [152] and $Rh/Fe(OH)_x$ [153] catalysts by a co-precipitation method, with high CO conversion efficiency near room temperature and tolerance to CO_2 and H_2O poisoning. L. Cao *et al.* adopted a reverse strategy by selectively and atomically dispersing $Fe(OH)_x$ species at the

surface of silica-supported Pt_{NP} through atomic layer deposition [154]. The catalyst achieved complete and 100% selective CO removal from -73 to 107 °C. From XAS, XPS, and DFT investigations, the PROX mechanism was suggested to involve Pt-$Fe_1(OH)_3$ interfacial sites, with COOH (resulting from CO+$Fe_1(OH)_3$ reaction) dehydrogenation to CO_2 as the rate-determining step. Note that this catalyst may also be seen as an SAA (Section 3.2) with dilute Fe atoms deposited onto Pt_{NP}. So do oxide-supported Pt-Fe nanoalloy catalysts prepared by Zhang *et al*., who also measured high PROX performance for this bimetallic system [155].

Even more recently, S. Cao *et al*. reported the preparation of a Pt SAC by incipient wetness impregnation of silica or alumina with an aqueous solution containing $H_2Pt(OH)_6$ as well as KOH or CsOH [156]. The alkali ions were assumed to stabilize Pt-$O(OH)_x$ species at the support surface, with good PROX performance around 100 °C. Here again, similar to what was previously proposed for supported gold nanocatalysts [157], surface hydroxyl groups (regenerated by O_2+H_2 reaction) are believed to play a prominent role as they open a faster CO oxidation pathway in the presence of H_2. This can be put in relation to the strong promoting effect of water reported for CO oxidation over a Pt/$Cr_{1.3}Fe_{0.7}O_3$ SAC [146] and ceria-supported SAC (Section 2.1.4). However, in these cases, the relevant reaction to be considered may be WGS.

2.3. Water-gas shift reaction (WGSR)

The WGSR ($CO + H_2O \leftrightarrow CO_2 + H_2$) is an important industrial process to produce CO-free hydrogen or to adjust the H_2/CO ratio required for Fischer-Tropsch and methanol synthesis [158–161]. The WGSR is thermodynamically more favorable at lower temperatures ($\Delta H_{298\,K}$ = -41.2 kJ mol^{-1}) and kinetically favored at high temperatures. Therefore, the reaction is industrially performed in several stages with different catalysts: the high-temperature shift

reaction is performed at 350−450 °C on iron-oxide-based catalysts, while the low temperature shift reaction is performed at 190−250 °C on copper-zinc-oxide-based catalysts. In the past two decades, noble-metal-based catalysts have been widely investigated for the WGSR due to their high stability and activity, and among them SAC have aroused great attention.

In 2003, the Flytzani-Stephanopoulos group reported the catalytic role of Au and Pt cations in WGSR [21]. Interestingly, the authors used a sodium cyanide leaching method to remove metallic NP contained in conventional Au/CeO_2 and Pt/CeO_2 catalysts. They found that their activity was almost unchanged, and concluded that only isolated metal cations or clusters strongly bonded to the support are the active sites. This has been debated since the activity of such catalysts could be modified by the presence of sodium cyanide (formation of $Na[Au(CN)_2]$), and Au/CeO_2 catalysts prepared by this method were less active than commercial $Cu/ZnO/Al_2O_3$, contrarily to other catalysts prepared by the deposition-precipitation method [162–165]. Furthermore, a precise comparison of the activity of the SA and NP active sites is not obvious.

The same group later showed that the introduction of alkali ions (sodium or potassium) can stabilize, at appreciable loading (ca. 1 wt%), atomically dispersed $Pt/Au\text{-}O_x(OH)\text{-}S$ sites (where S is the oxide support), which are able to catalyze the WGSR at low temperature (<250 °C) [166–170]. Alkali cations were reported by Ammal and Heyden to behave similarly as reducible oxide supports by supplying OH species for the WGSR and activating H_2O molecules [171]. In a study by the Stair group, high-angle annular dark field (HAADF) STEM images confirmed the higher dispersion of Pt in $Pt\text{-}Na/SiO_2$ as compared to Pt/SiO_2. However, CO-FTIR data revealed that the promotional effect of Na^+ in the WGSR mainly originates from an alteration of the properties of Pt_{NP}, not Pt_{SA} [172].

Au_{SA} and Pt_{SA} supported on CeO_2 as well as TiO_2, SiO_2, FeO_x, MnO_x and inert KLTL zeolites, were later proposed by several groups to be the active sites in the WGSR [173,174]. As shown

in **Figure 6**, the TOF are similar on different supports, and only specific to the nature of the metal cation of the active site, *i.e.* Au(I) (45 ± 5 kJ/mol) or Pt(II) (70 ± 10 kJ/mol) [175]. However, by using CO-FTIR spectroscopy to distinguish Pt_{SA} from Pt_{NP}, the Stair group concluded that Pt_{SA} in Pt/H-ZSM5 and Pt/SiO_2 catalysts behave as spectators for the WGSR, unlike Pt_{NP} [172]. Their low catalytic activity was attributed to the strong binding of CO molecules.

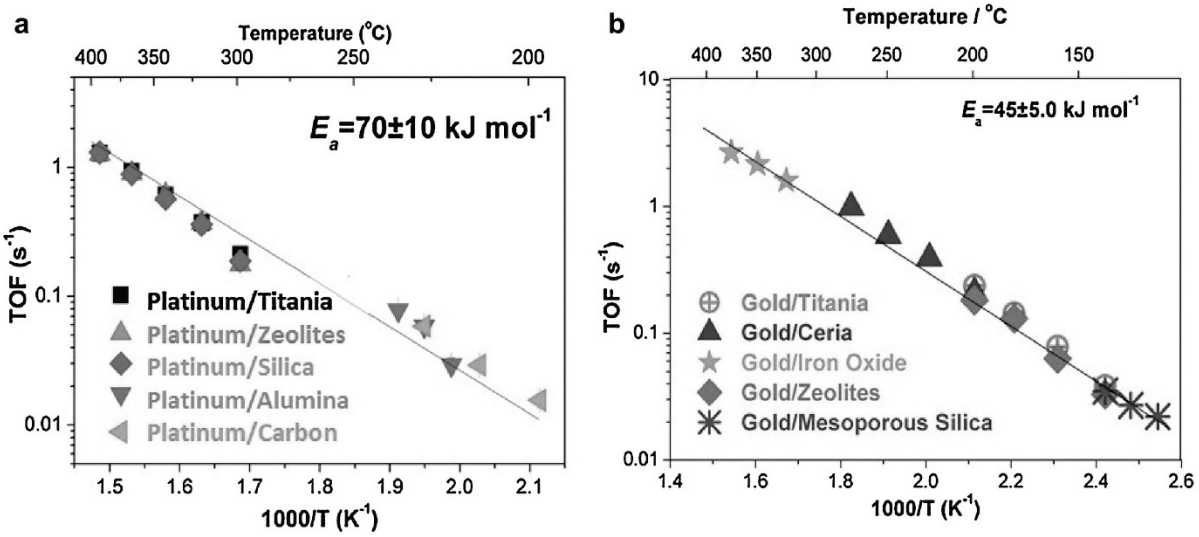

Figure 6. a) TOF of the WGSR on Na-containing Pt catalysts on various supports in a simulated reformate-gas mixture ($CO:H_2O:CO_2:H_2$ = 11:26:7:26 vol%); **b)** TOF plot for the WGSR over atomically dispersed gold catalysts in the same mixture. Adapted with permission from [175], Copyright 2017 Elsevier.

The role of support nanostructuring was also investigated. Ceria nanorods exhibiting {110} and {100} crystal surfaces stabilize gold as single atoms and clusters (<1 nm), while Au_{NP} (~3 nm) were present on the {100} facets of ceria nanocubes. The activities of Au/CeO_2 nanorods were found at least one order of magnitude higher for the WGSR and steam reforming of methanol at low temperatures [176]. Furthermore, hollow mesoporous CeO_2 microspheres with a high surface area and a mesoporous structure were shown to stabilize single Au atoms catalyzing the

WGSR with higher performances than those obtained using ceria synthesized through co-precipitation and sol-gel methods [177].

High WGSR performances were also reported for SAC containing other elements than Au or Pt. For instance, the catalytic activity of a 0.37 wt% Rh_{SA}/TiO_2 catalyst was around four times higher than that of a Rh/TiO_2 nanocatalyst, without any methanation at 300 °C, even under CO_2- and H_2-rich WGSR stream. The suppression of methanation was attributed to the absence of H_2 dissociative adsorption on Rh_{SA}/TiO_2 [178]. The activities of Ir/FeO_x [179] and Pd/FeO_x [180] SAC were one order of magnitude higher than those of their cluster or NP counterparts. This better performance was ascribed to the enhanced reducibility of the FeO_x support, and the generation of O_v that promote the dissociation of H_2O to form H_2 and atomic oxygen.

Environmental STEM in controlled WGS atmospheres revealed the formation of clusters of only a few gold atoms resulting from SA dynamics, and the catalytic effect of low-coordination surface sites [181]. Conversely, Pd can be predominantly dispersed as isolated atoms onto TiO_2 during the reverse-WGSR at 400 °C. The thermodynamic stability of Pd was associated with Pd-Ti coordination (as evidenced by EXAFS), which manifests upon O_v formation [182].

A major difference in reaction mechanisms between SA and NP was highlighted for Pt/FeO_x catalysts [183]: on Pt_{NP}, CO is strongly adsorbed and reacts with OH groups, leading to formates, which then decompose to simultaneously produce CO_2 and H_2. On Pt_{SA}, adsorbed O species formed by dissociation of H_2O on O_v of FeO_x combine with weakly adsorbed CO to produce CO_2. The activation energy of this process is only 33 kJ/mol, *vs* 61 kJ/mol for Pt_{NP}/FeO_x catalysts. A similar redox mechanism was reported for Pd_{SA}/FeO_x, with also a low activation energy of ca. 30 kJ/mol [180]. A specific redox mechanism, involving electron transfer from Fe^{3+}-O$\cdots$$Ir^{2+}$-$O_{vac}$ to Fe^{2+}-$O_{vac}\cdots Ir^{3+}$-O (dual metal active site), was proposed for Ir_{SA}/FeO_x from a theoretical and experimental study: H_2O dissociates to OH on Ir_{SA}, and to H on the first-neighbor O atom bonded with an Fe site [184]. CO adsorbed on Ir_{SA} reacts with

another adjacent O species to produce CO_2, yielding an O_v. H_2 is then formed by migration of H from adsorbed OH toward Ir_{SA}, and its subsequent reaction with another H.

2.4. Total oxidation of hydrocarbons

Catalytic reactions consisting of hydrocarbon total oxidation are useful in a range of energy generation devices such as gas turbines and heating systems, and environmental applications such as the purification of indoor air, outdoor air, and vehicle exhaust. In 1999, Iwasawa and coworkers reported an EXAFS investigation of atomically dispersed Pt and $PtMo_6$ species on MgO prepared by impregnation-calcination, forming a spinel-like distorted structure [18]. These catalysts were found to be as active as MgO-supported metallic Pt particles for propane combustion. Single Pt ions could be converted into Pt_6 clusters upon a propane reducing treatment, and regenerated back upon O_2 calcination at 450 °C. Recently, Wang *et al*. showed that a Pt/La-Al_2O_3 SAC was active for the propene combustion [63]. The authors found that the Pt atoms remained isolated if, and only if, oxidic Ba species were additionally introduced in the preparation. A number of SAC studies have also been devoted to methane oxidation. Tang *et al*. prepared Pt-doped CeO_2 catalysts by several methods and found that the rate of methane partial oxidation with CO_2 (to CO) and total oxidation with O_2 (to CO_2) increases with the fraction of ionic Pt sites [23]. From DFT calculations, it was suggested that the dissociative adsorption of methane is the rate-determining step, which is favored at the surface in the vicinity of Pt dopants, where O atoms are more labile. In contrast to these results, Jeong *et al*. recently found that highly oxidized Pt SAC are less active for methane oxidation as well as CO and NO oxidation than Pt_{NP} catalysts, which are themselves less active than metallic Pt SAC [116]. The Pt oxidation state, which would be barely changed upon the reactions, could be controlled by using as support defective ceria islands at an alumina surface, and by varying the catalyst prereduction temperature. Yan *et al*. reported an original strategy to synthesize a thermally

stable Pt_{SA}/Mn_2O_3 catalyst for methane combustion [185]. Platinum was preloaded as SA on Mn_3O_4 through a redox precipitation method, and the resulting SAC precursor was calcined in humid air (3 vol% H_2O) at 800 °C for five days. This led to the strong anchoring of single Pt^{4+} atoms onto the reconstructed Mn_2O_3 phase, which was further optimized by H_2O_2 etching of the oxide surface. Besides Pt-based SAC, Pd atomically dispersed on oxides was also found efficient for methane and toluene combustion [75,186]. Overall, it is often pointed out that the supports play a role as important as that of the metal atoms [75], which in some cases only have a promoting effect on the inherent oxidation activity of the oxides [185].

Manganese oxide was also used as a SAC support by Tang and coworkers in the form of microporous hollandite Mn oxide (HMO) nanorods. Silver atoms could be anchored at the pore openings of HMO(001) facets, and the resulting catalyst was active for the combustion of volatile organic compounds such as formaldehyde [187] and benzene [188]. Surprisingly, the replacement of Ag with Na located at similar sites of HMO led to enhanced formaldehyde abatement performance, which was ascribed to an increased electron density of neighboring surface lattice oxygen atoms with respect to Ag/HMO [189]. Hence, the role of the alkali metal could be more than that of a promoter, as it was previously believed from the high performance of an atomically dispersed Na-promoted Pt/TiO_2 catalyst for the total oxidation of formaldehyde [190]. Potassium-loaded hollandite-type MnO_2 and TiO_2 structures were also found efficient for diesel soot oxidation [191]. Still with Mn oxide, Zhang *et al*. prepared a SAC consisting of Pt_{SA} on defective MnO_2 nanosheets through a one-pot hydrothermal method for low-temperature toluene oxidation [192]. Original strategies were also employed for the preparation of SAC for the oxidative removal of benzene, whether on $Pd/CuO/\gamma\text{-}Al_2O_3$ prepared by galvanic replacement [193] or on Pt-loaded ordered mesoporous Fe_2O_3 [194]. For the latter, the authors found enhanced activity and stability with respect to supported NP. The superiority of Pt_{SA} was

also reported for the total oxidation of methanol over Pt/Co_3O_4 [195] and of butanone on Pt/WO_3 [196].

2.5. Selective oxidation reactions

2.5.1. Early transition metals on oxides

Site isolation, which corresponds to the spatial separation of active sites at the surface of heterogeneous catalysts, is a key parameter in selective oxidation (SELOX) reactions to avoid deep oxidation (formation of CO_x) and obtain high selectivity to partial oxidation products [197–199]. This concept was formulated in the early 1950s by Grasselli, and was defined as one of the seven pillars in SELOX [198]. Since then, it has been widely applied both to bulk oxides and supported early transition metals such as V, Mo, Ti, and Cr.

Various methods, such as impregnation at low metal loading, co-condensation [200], thermolytic molecular precursor method [201–204], cation immobilization by amino groups [205], and flame pyrolysis [206], have been developed to isolate supported active sites, also called monomeric sites. This has led to high selectivities in various reactions such as oxidative dehydrogenation of methanol [201], epoxidation of cyclohexene [202,207], hydroxylation of benzene [206], and photo-assisted epoxidation of styrene [208]. In particular, VO_x/SiO_2 catalysts were applied to challenging reactions such as (photo)catalytic oxidation of methane to methanol and formaldehyde [200,204,209,210] and oxidative dehydrogenation of propane [206,211–213], during which CO_x species are very easily produced.

The molecular structure of these isolated sites was characterized by vibrational spectroscopies (especially Raman for iono-covalent oxides) [200,202,204,205,214,215], UV-Vis spectroscopy [202–205,208,210,211,216,217], electron spin resonance spectroscopy [200,205,211,216], and

EXAFS [201,206]. The need for *in situ* techniques quickly became evident since the structure of supported oxometallates strongly depends on their environment. For instance, polyoxometalates supported on silica, which are stable in hydrated conditions (e.g. in ambient air), decompose upon dehydration at elevated temperature, leading to isolated species [214,218]. The role of bridging bonding with the support and of the support itself was also investigated. Khaliullin *et al.* reported that the TOF of methanol oxidation to formaldehyde is more than 100 times greater for VO_x/TiO_2 and VO_x/ZrO_2, than for VO_x/SiO_2 [219]. The authors proposed that formaldehyde formation from methoxy groups may require pairs of adjacent VO_4 groups or V_2O_5 dimers. For propane oxidative dehydrogenation to propylene, the TOF of VO_x/ZrO_2 catalysts was found almost independent on the surface vanadia coverage (*i.e*. similar for monomeric and polymeric vanadia species) [220]. This suggests that the reaction requires only one surface VO_4 group. However, the propylene selectivity increases with increasing surface vanadia loading, which was explained by the removal of unselective Zr–OH groups upon vanadia deposition. Finally, the role of support defects was underlined. For example, Launay *et al*. proposed that hydrolyzed D2 defects in SiO_2 would act as preferential anchoring sites for monomeric hydroxylated species, which are the most efficient ones for the SELOX of methane [214,215].

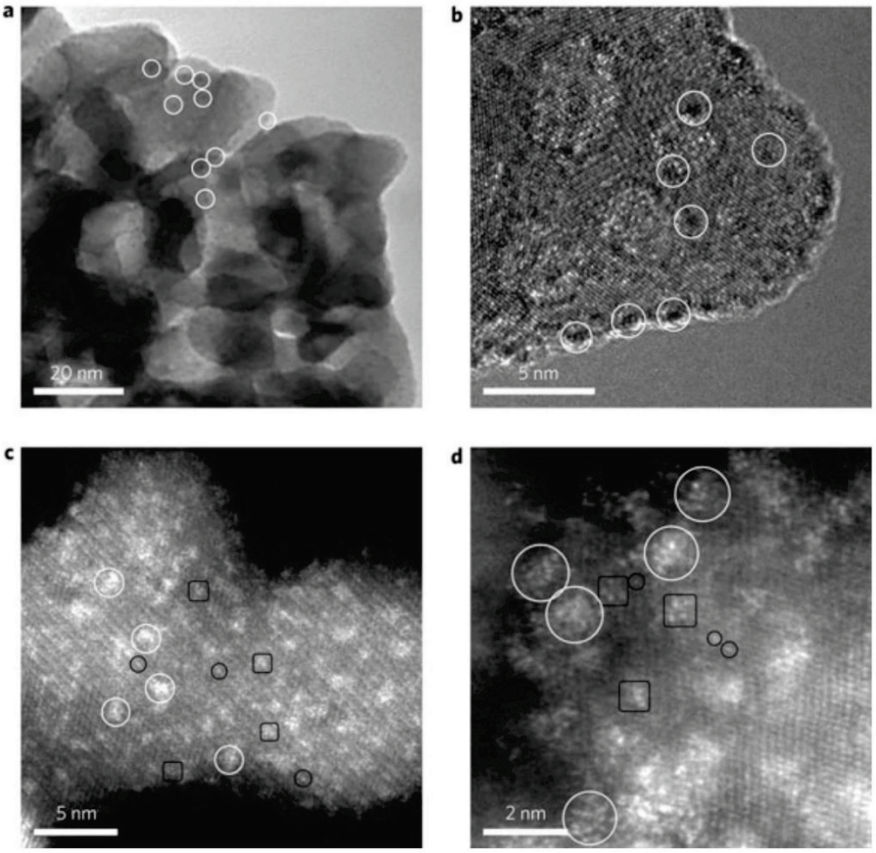

Figure 7. TEM **(a)**, HRTEM **(b)** and HAADF-STEM **(c,d)** images of a WO_x/ZrO_2 sample. Black circles indicate the presence of single W atoms corresponding to surface mono-tungstate species. Black squares indicate surface poly-tungstate species with several W atoms linked by oxygen bridging bonds. White circles indicate WO_x clusters with diameters of ~0.8–1.0 nm. Reproduced with permission from [221], Copyright 2009 Springer Nature.

Progress in electron microscopy has allowed the direct visualization of monomeric and polymeric species [221–224], as illustrated in **Figure 7** by HAADF-STEM images of WO_x/ZrO_2, which is a solid well known for its acidic properties, but is also efficient for some SELOX reactions [225,226]. It has also led to a change of terminology in the community working on selective oxidation. For instance, one can find the term “single Cr atoms” in the recent literature [227].

2.5.2. Late transition metals on oxides

SAC such as Pd_{SA}/silicate [228] and Rh_{SA} on ZrO_2 [229], TiO_2 [230], ZSM-5 zeolite [230], or CeO_2 [231], were shown to be efficient for the SELOX of methane in aqueous solution using either H_2O_2 or O_2 as oxidant. For Rh_{SA}/ZrO_2, DFT calculations indicate that four-coordinated Rh atoms stabilize CH_3 species by suppressing further dehydrogenation, unlike five-coordinated Rh atoms [229,232]. Rh_{SA} also facilitate the activation of H_2O_2 and the formation of the CH_3OOH intermediate. The spontaneous dissociative adsorption of H_2O_2 on Rh_{SA}/ZrO_2 was reported to form an O_2Rh active site and to hydrogenate the surrounding ZrO_2 surface [233]. After the adsorption of CH_4 on O_2Rh/ZrO_2-2H, the C−H bond is activated by H abstraction with a barrier of 1.23 eV, leading to a methyl radical and the hydrogenated HOO-Rh species. Adsorbed CH_3 can further react with HOO-Rh to produce CH_3OH with a barrier of 0.30 eV. After desorption of CH_3OH, a second methane molecule can be adsorbed on the ORh/ZrO_2-2H site, which is easily activated (barrier of 0.60 eV) to form CH_3. The second CH_3OH molecule is then produced with a barrier of 0.39 eV. In the case of Rh_{SA}/ZSM-5, the oxidative addition pathway for the activation of methane occurs at coordinately unsaturated Rh atoms, with a very low barrier of 0.07 eV for Rh(CO) [234]. The rate-determining step corresponds to the formation of a C–OH bond, which is promoted by CO coordinated to Rh. Finally, water was shown to prevent poisoning by CO, and to protonate an intermediate RhOOH species.

As compared to their NP counterparts, several SAC exhibited a higher activity for the SELOX of alcohols with molecular oxygen, which was ascribed to their maximal number of interfacial sites [235]. Their higher selectivity was explained by the activation of lattice oxygen at the interface. Similarly, Au_{SA}/SiO_2 catalysts prepared by cyanide leaching were found to be very active for the solvent-free aerobic oxidation of benzyl alcohol to benzaldehyde [236]. Their activities were measured to be identical to those of the unleached catalysts, and TON values

higher than 4×10^5 h^{-1} were obtained based on the Au content. 100% selectivity below 180 °C and high stability for ten hours was reported for methanol dehydrogenation to produce methyl formate and H_2 on Na^+- stabilized Au_{SA}/TiO_2 prepared by incipient wetness impregnation of Au_{SA}-O_x-Na_9-$(OH)_y$ solutions [237]. Pd/SiO_2 and Cu/SiO_2 catalysts containing metal NP are unselective and inactive, respectively, for this reaction. Interestingly, 92% selectivity to methyl formate at 65% conversion and high stability for ten hours were obtained with a $Pd_{0.01}Cu/SiO_2$ SAA catalyst (Section 3.2) prepared by adding a small amount of Pd onto Cu NP [238]. Pd_{SA}/Al_2O_3 exhibited quite high performance in the aerobic SELOX of cinnamyl and crotyl alcohols under mild conditions [17], though with a lower selectivity to the α,β-unsaturated carbonyl compound (~90%) than state-of-the-art supported Au catalysts [239]. In the case of SELOX of cinnamyl alcohol, the TOF of Pd^{II} isolated sites is 4400 h^{-1} at 60 °C, against 538 h^{-1} at 120 °C for Au/CeO_2 catalysts. For the SELOX of crotyl alcohol, the TOF is one order of magnitude higher than that of surface PdO_x species, while a high selectivity is retained [17]. In another study, a Pd_{SA}/Al_2O_3 catalyst showed higher activity and selectivity as compared to Pd_{NP} for the oxidation of cinnamyl alcohol [240]. This work also highlighted the key role of coordinately unsaturated Al^{3+} sites in trapping Pd atoms and tuning their electronic properties. It was also concluded that oxygen species formed by the interaction of O_2 with Pd_{SA}/Al_2O_3 oxidize the partially dehydrogenated intermediates to cinnamaldehyde. Pd_{SA}/TiO_2 was reported to catalyze the epoxidation of light olefins (except ethylene) in the presence of O_2 and H_2 at room temperature [241]. However, one can note that the yields were quite low (*e.g.* 1-2% for propene to propylene oxide). 91% conversion of 5-hydroxymethylfurfural and 81% selectivity to 2,5-diformylfuran for 2 h at 110 °C were obtained with a Ru_{SA}/NiO catalyst prepared by a ball-milling method [242]. Finally, $Rh_{SA}/ZSM\text{-}5$ was found efficient to convert CH_4 to acetic acid and methanol through coupling of CH_4, CO and O_2 in solution below 150 °C [243]. Computational studies suggested that CH_4 is activated by Rh_1O_5 anchored on the wall of

micropores of the ZSM-5 zeolite. The resulting CH_3 then couples with CO and OH to produce acetic acid with a low activation barrier.

3. Single-atom catalysts supported on carbon and other materials

SAC supports are not limited to oxides and zeolites, and support materials such as metal-organic frameworks [244,245] or sulfides [246] have been investigated for selective oxidation. Here we briefly report on two important catalyst types, namely carbon-based SAC and SAA.

3.1. Carbon and nitrogen-hosted SAC

Besides oxide-supported SAC for gas-phase thermal oxidation reactions, carbon-based materials are by far the most widely employed SAC supports or hosts for applications in liquid-phase electrocatalysis, photocatalysis, and hydrogenation or coupling thermocatalysis [247]. Among other advantages, one can cite the beneficial properties of carbon (graphite, graphene, carbon nanotubes, activated carbon, etc.) in terms of specific surface area, electrical and thermal conductivities, and tunable surface functionalization (see Chapter 3). Doping of carbon with nitrogen or using a carbon nitride such as graphitic C_3N_4, allows for the stabilization of noble and non-noble metals in an isolated form through several metal-nitrogen bonds [2]. A number of studies have investigated the catalytic thermal oxidation properties of carbon-supported SAC, most often under mild liquid-phase conditions.

3.1.1. Selective oxidation of alcohols

Li and coworkers reported the preparation of a Co-N-G (N-doped graphene) SAC by heat treatment of cobalt salts and graphene oxide in ammonia atmosphere [248]. The catalyst showed high stability and atom efficiency for the selective aerobic oxidation of benzyl alcohol and derivatives to the corresponding aldehydes. For benzyl alcohol, the achieved conversion was

94.8% with 97.5% benzaldehyde selectivity. Xie *et al*. further reported that all M-N-C (M = Fe, Co, Ni, Cu, Cr) SAC – synthesized by pyrolysis of metal nitrate and nicarbazin – are able to catalyze benzyl alcohol oxidation to benzaldehyde, Cu-N-C being the most efficient system [249]. In addition, Fe-N-C was found active for the aqueous-phase aerobic oxidation of 5-hydroxymethylfurfural to 2,5-diformylfuran. In comparison, the oxidation of aliphatic alcohols (ethanol, 1,6-hexanediol, glycerol) was found much less efficient.

Ding *et al*. designed a SAC consisting of an Fe-based polymerized ionic liquid monolayer on carbon nanotubes (CNT), which exhibited more than 99% regioselectivity for phenol hydroxylation to catechol (1,2-dihydroxybenzene) with hydrogen peroxide, and an activity superior to that of its homogeneous free ion counterpart [250]. As suggested by experimental and theoretical investigations, the Fe atom would coordinate to four oxygen atoms at the CNT surface, and the reaction mechanism would involve the non-radical addition of an OH group at the *ortho*-carbon atom of phenol through the formation of a ferric-hydroperoxo complex.

3.1.2. Selective oxidation of hydrocarbons

Liu *et al*. prepared Fe-N-C SAC by an MgO template-sacrificial pyrolytic approach, which exhibited high room-temperature activity, selectivity, and reusability for the C-H bond oxidation in a number of substrates – including ethylbenzene toward acetophenone – dissolved in an aqueous solution of *tert*-butyl hydroperoxide [251]. Using STEM, XPS, XAS, electron spin resonance spectroscopy, Mössbauer spectroscopy and KSCN titration experiments, the authors showed that the pyrolysis temperature (600-800 °C under N_2 atmosphere) controls the relative concentrations of FeN_x species (x = 4-6) coexisting in the SAC, which in turn critically affect the reaction TOF in this order: $Fe^{III}N_5 > Fe^{III}N_6 > Fe^{II}N_4$.

Bakandritsos *et al*. reported the beneficial influence of mixed valence for Cu atoms anchored onto graphene functionalized with nitrile groups (cyanographene) to reach near 100%

conversions and selectivities for the aerobic oxidation of benzylic C-H bonds and the oxidative coupling of amines toward pharmaceutical synthons [252]. These high performances were explained by a short-distance cooperative synergy between Cu(II) and Cu(I) species (cyanographene allows the partial reduction of Cu(II) to Cu(I)), as observed in metalloenzymes).

Acetophenone could also be synthesized with high yield and regioselectivity from aryl alkenes – including styrene – through the Wacker-type aerobic oxidation using isopropanol as the hydrogen source and a Co-N-C SAC prepared by impregnation-pyrolysis [253]. The corresponding industrial process, which uses catalytic $PdCl_2$ and stoichiometric $CuCl_2$, has a number of limitations, which makes the SAC an elegant alternative.

Zhang *et al*. anchored Cu atoms in Cu-N_3 coordination onto porous hollow graphitic carbonitride spheres synthesized using a template-free preassembly strategy, which exhibited high conversion and higher selectivity and stability than Cu_{NP} for the oxidation of benzene to phenol [254]. The Fe-N-C system was also reported to be efficient for this reaction, while Fe_{NP} counterparts showed lower conversion and selectivity [255,256]. Noticeably, Deng *et al*. were able to directly reveal the atomic structure of FeN_4 centers embedded in graphene by combining STEM and STM methods [255].

3.1.3. Other reactions

Another reaction in which a SAC was found much more efficient than its homogeneous or nanoparticulate counterparts is the gold-catalyzed selective oxidation of silanes to silanols using water, as reported by Chen *et al*. for Au_{SA} anchored through three bonds onto mesoporous polymeric graphitic carbon nitride (mpg-C_3N_4) [257].

The use of SAC was also found beneficial to reactions involving hydrogen peroxide, such as the direct synthesis of H_2O_2 from H_2 and O_2 over atomically dispersed $PdCl_x$/C [258], and the

peroxone reaction between O_3 and H_2O_2 – for hydroxyl radical generation in acid solution – over Mn-N_4 sites dispersed in g-C_3N_4 [259]. Similarly, a Cu-C_3N_4 SAC was recently found efficient for the activation of H_2O_2 to hydroxyl radicals (Fenton reaction) and subsequent oxidative degradation of rhodamine B, in the context of organic wastewater treatment [260]. SAC such as Fe- and Cu-N-C were also reported to exhibit enzyme-like activity ("SA nanozymes") in e.g. (per)oxidase-catalyzed reactions [261,262].

The excellent activity as well as steam and sulfur-resistance of the emblematic Fe-N-C system – consisting here of Fe-N_4 centers confined in polymeric carbon nitride through a copolymerization approach – for gas-phase H_2S oxidation into elemental sulfur was recently reported by Lei *et al*. [263]. Based on DFT calculations, the authors propose H_2S and O_2 dissociative adsorptions at (probably separate) Fe-N_4 centers, leading to HS-Fe-N_4 and O* radical species, which in turn exothermally generate S and H_2O (**Figure 8a**).

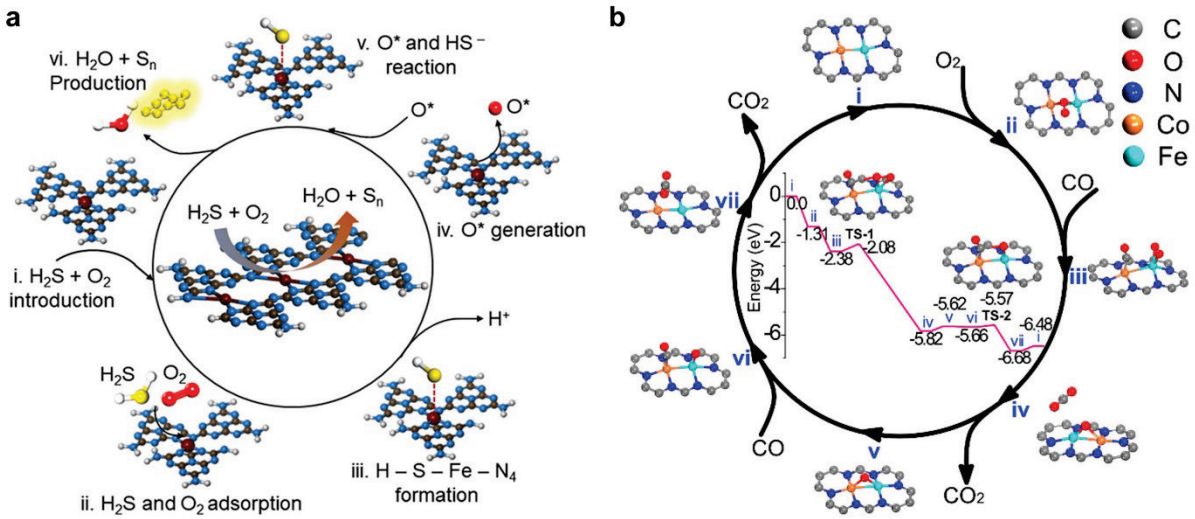

Figure 8. DFT calculation-based reactions schemes. **a)** H_2S oxidation on Fe-N_4-carbon nitride. Reproduced with permission from [263], Copyright 2020 Wiley-VCH. **b)** CO oxidation on Fe-Co-N-C. Adapted with permission from [264], Copyright 2020 ACS.

Finally, CO oxidation, the usual gas-phase test reaction, was also carried out on carbon-based SAC. In particular, these supports materials are ideally suited to elaborate bimetallic "double-atom catalysts" (see Chapter 15) and explore the catalytic performance of neighboring metal elements. Zhou *et al*. reported the stabilization of Pt-Ru dimers by forming Pt–C and Ru–N bonds in the triangular cavities of N-deficient g-C_3N_4 through an icing-assisted photocatalytic reduction method, leading to improved CO oxidation activity with respect to monometallic SA and double-atom counterparts [265]. Wang *et al*. synthesized a single-site catalyst consisting of N-coordinated Fe-Co dimers in a carbon matrix from the pyrolysis of an Fe-impregnated Zn/Co metal-organic framework, leading to CO oxidation activity at a temperature as low as -73 °C [264]. From *in situ* XAS, pulse-adsorption microcalorimetry, and DFT, the authors concluded that the reaction proceeds through the LH mechanism, with CO and O_2 preferentially adsorbing on Co and Fe atoms, respectively (**Figure 8b**).

3.2. Single-atom alloy catalysts

Single-atom alloys [34,266], which were previously referred to as site/atom-isolated or ultralow-loading alloys, can also be considered as SAC. They consist of isolated atoms of a metal at the surface of another metal, which is either in the form of an extended single crystal or of (supported) NP. The metal phase can be an intermetallic compound such as $Al_{13}Fe_4$ [267], or an alloy such as Ag-Cu dilute in Cu [268]. Although the SAA strategy is interesting to isolate active centers and tune their electronic structure, it has rarely been applied – at the notable exception of Au-Pd alloys – to oxidation reactions. One of the main reasons is the potential poisoning of the more active dopant atom in oxidative environments – *e.g*. O-Pd-O – which may render the dopant atom inactive. Several surface-science or powder-catalyst studies focused on CO oxidation over Au-Pd alloys dilute in Pd [269–272]. A matter of debate is the need for contiguous Pd surface atoms in the dissociative adsorption of O_2 and its reaction with CO through the LH mechanism. Ouyang *et al*. examined hydrogen peroxide synthesis from

hydrogen oxidation over Au-Pd/TiO_2 catalysts [273]. Isolated Pd atoms were assumed to be active and selective sites for H_2O_2 formation, while contiguous Pd ensembles would be unselective, *i.e.* catalyze H_2O formation. Zhang *et al*. reported enhanced glucose oxidation performances for colloidal Au-Pd NP presenting dilute, low-coordinated and negatively charged surface Au atoms [274]. Sun et al. found that photodepositing 0.05 wt% site-isolated Pd at the surface of 0.94 wt% Au_{NP} on TiO_2 was enough to reach a maximum activity for the aerobic solvent-free oxidation of benzyl alcohol to benzaldehyde [275]. The reader is referred to Chapter 4 of this book for more information on SAA catalysts.

4. Summary and conclusions

A number of thermal oxidation reactions have been investigated over SAC, CO oxidation being by far the most studied one. A large part of this chapter has attempted to review the knowledge on the structure, performance, and CO oxidation mechanism of late transition metal atoms supported on various oxides. The latter part of the chapter highlighted interesting properties of SAC in PROX, WGS, and hydrocarbon combustion as well. In addition, oxometallate monomers supported on oxides and single metal atoms stabilized in N-doped carbon or carbon nitride are efficient for gas-phase and liquid-phase selective oxidations, respectively.

For the important aspect of SAC stability (both in terms of atom isolation and catalytic performance), it is possible to rank the metal/oxide systems as a function of the metal element across the periodic table and the reducibility of the oxide. While early transition metals supported on reducible oxides will typically remain isolated owing to stabilizing oxo bridges, noble metals supported on non-reducible oxides are prone to diffusion and aggregation. Moreover, highly oxidizing reaction conditions are much more favorable to metal atom anchoring and isolation than reducing ones. In order to avoid metal atom clustering, a frequent approach has initially consisted in the use of very low metal loadings, which does not avoid

surface diffusion but considerably reduces the probability of multimer formation by reducing the metal atom collision frequency. Complementary approaches use tiny support particles or strongly anchoring oxide patches onto a high-surface area support (*e.g*. CeO_2/Al_2O_3) for trapping SA. In addition, recent SAC design strategies rely on the stabilization of SA on their support or in their host through defect engineering or doping, as in the case of N-doped carbons.

Provided the stability criterion is fulfilled, another important question arises concerning the oxidation activity of SAC compared to nanocatalysts. The previous review of the literature for metal/oxide SAC shows that the answer not only depends on the considered catalytic system, but sometimes also on the initial oxidation state of the SA. In some cases, SAC have been reported to be inactive, whereas their supported cluster or NP counterparts are efficient. Thus, SAC should not be considered as the universal panacea. Beyond the possible decrease in metal content, prominent advantages of supported SAC lie in their potential to replace homogeneous catalysts (heterogenization) or noble-metal-based heterogeneous catalysts (metal substitution) in selected reactions. Promising results have been reported in that regard, and plausible reaction mechanisms – often involving O_v and the MvK mechanism for oxide-supported SAC – have been suggested. However, to go further, we believe that the SAC community urgently needs more systematic studies, *e.g*. by comparing several metals, both in the SA and NP forms, for a given support and reaction, together with in-depth characterization at least before and after reaction, if not *operando* (which is particularly relevant as the state of metal species dynamically responds to the chemical environment). This will guide theoretical modeling, which in turn will be in position to predict efficient SAC. This holds especially true for non-noble transition metals, which have been comparatively little investigated owing to their challenging preparation and characterization.

A final challenge faced in developing a predictive theory of SAC performance with variation in the metal and support composition is metal and support-dependent differences in the active

site coordination environment. For example, if one assumes that Pt^{2+} prefers to exist in a four-fold square planar coordination to an oxide support, then the question is whether the support surface can allow this. For CeO_2 the answer seems to be yes, while for TiO_2 the geometry forms via additional OH species creating a strained 4-fold coordination. Thus, the preferred coordination environment of each metal and each support is likely to be different, based on well-known coordination preferences from inorganic chemistry and the accessibility of these structures on a specific surface, making the existence of clear trends more challenging than for extended metal surfaces. This increased complexity, however, also presents increased opportunity for controlling catalytic functionality!

5. References

[1] Liu, J. Catalysis by Supported Single Metal Atoms. *ACS Catal.*, **2017**, *7*, 34–59.

[2] Mitchell, S.; Vorobyeva, E.; Pérez-Ramírez, J. The Multifaceted Reactivity of Single-Atom Heterogeneous Catalysts. *Angew. Chem. Int. Ed.*, **2018**, *57*, 15316–15329.

[3] Zhang, H.; Liu, G.; Shi, L.; Ye, J. Single-Atom Catalysts: Emerging Multifunctional Materials in Heterogeneous Catalysis. *Adv. Energy Mater.*, **2018**, *8*, 1701343.

[4] Yan, H.; Su, C.; He, J.; Chen, W. Single-Atom Catalysts and Their Applications in Organic Chemistry. *J. Mater. Chem. A*, **2018**, *6*, 8793–8814.

[5] Cui, X.; Li, W.; Ryabchuk, P.; Junge, K.; Beller, M. Bridging Homogeneous and Heterogeneous Catalysis by Heterogeneous Single-Metal-Site Catalysts. *Nat. Catal.*, **2018**, *1*, 385–397.

[6] Wang, A.; Li, J.; Zhang, T. Heterogeneous Single-Atom Catalysis. *Nat. Rev. Chem.*, **2018**, *2*, 65–81.

[7] Zhang, L.; Ren, Y.; Liu, W.; Wang, A.; Zhang, T. Single-Atom Catalyst: A Rising Star for Green Synthesis of Fine Chemicals. *Natl. Sci. Rev.*, **2018**, *5*, 653–672.

[8] Liu, J.; Bunes, B.R.; Zang, L.; Wang, C. Supported Single-Atom Catalysts: Synthesis, Characterization, Properties, and Applications. *Environ. Chem. Lett.*, **2018**, *16*, 477–505.

[9] Li, X.; Yang, X.; Huang, Y.; Zhang, T.; Liu, B. Supported Noble-Metal Single Atoms for Heterogeneous Catalysis. *Adv. Mater.*, **2019**, *31*, 1902031.

[10] H Sykes, E.C.; Christopher, P. Recent Advances in Single-Atom Catalysts and Single-Atom Alloys: Opportunities for Exploring the Uncharted Phase Space in-Between. *Curr. Opin. Chem. Eng.*, **2020**, *29*, 67–73.

[11] Kaiser, S.K.; Chen, Z.; Faust Akl, D.; Mitchell, S.; Pérez-Ramírez, J. Single-Atom Catalysts across the Periodic Table. *Chem. Rev.*, **2020**, *120*, 11703–11809.

[12] Thomas, J.M.; Raja, R.; Lewis, D.W. Single-Site Heterogeneous Catalysts. *Angew. Chem. Int. Ed.*, **2005**, *44*, 6456–6482.

[13] Copéret, C.; Comas-Vives, A.; Conley, M.P.; Estes, D.P.; Fedorov, A.; Mougel, V.; Nagae, H.; Núñez-Zarur, F.; Zhizhko, P.A. Surface Organometallic and Coordination

Chemistry toward Single-Site Heterogeneous Catalysts: Strategies, Methods, Structures, and Activities. *Chem. Rev.*, **2016**, *116*, 323–421.
[14] Samantaray, M.K.; D'Elia, V.; Pump, E.; Falivene, L.; Harb, M.; Ould Chikh, S.; Cavallo, L.; Basset, J.-M. The Comparison between Single Atom Catalysis and Surface Organometallic Catalysis. *Chem. Rev.*, **2020**, *120*, 734–813.
[15] Yang, C.; Garland, C.W. Infrared Studies of Carbon Monoxide Chemisorbed on Rhodium. *J. Phys. Chem.*, **1957**, *61*, 1504–1512.
[16] Wovchko, E.A.; Yates, J.T. Activation of O2 on a Photochemically Generated RhI Site on an Al2O3 Surface: Low-Temperature O2 Dissociation and CO Oxidation. *J. Am. Chem. Soc.*, **1998**, *120*, 10523–10527.
[17] Hackett, S.F.J.; Brydson, R.M.; Gass, M.H.; Harvey, I.; Newman, A.D.; Wilson, K.; Lee, A.F. High-Activity, Single-Site Mesoporous Pd/Al2O3 Catalysts for Selective Aerobic Oxidation of Allylic Alcohols. *Angew. Chem. Int. Ed.*, **2007**, *46*, 8593–8596.
[18] Asakura, K.; Nagahiro, H.; Ichikuni, N.; Iwasawa, Y. Structure and Catalytic Combustion Activity of Atomically Dispersed Pt Species at MgO Surface. *Appl. Catal. A*, **1999**, *188*, 313–324.
[19] Abbet, S.; Sanchez, A.; Heiz, U.; Schneider, W.-D.; Ferrari, A.M.; Pacchioni, G.; Rösch, N. Acetylene Cyclotrimerization on Supported Size-Selected Pdn Clusters ($1 \leq n \leq 30$): One Atom Is Enough! *J. Am. Chem. Soc.*, **2000**, *122*, 3453–3457.
[20] Abbet, S.; Heiz, U.; Häkkinen, H.; Landman, U. CO Oxidation on a Single Pd Atom Supported on Magnesia. *Phys. Rev. Lett.*, **2001**, *86*, 5950–5953.
[21] Fu, Q.; Saltsburg, H.; Flytzani-Stephanopoulos, M. Active Nonmetallic Au and Pt Species on Ceria-Based Water-Gas Shift Catalysts. *Science*, **2003**, *301*, 935–938.
[22] Aguilar-Guerrero, V.; Gates, B.C. Kinetics of CO Oxidation Catalyzed by Highly Dispersed CeO2-Supported Gold. *J. Catal.*, **2008**, *260*, 351–357.
[23] Tang, W.; Hu, Z.; Wang, M.; Stucky, G.D.; Metiu, H.; McFarland, E.W. Methane Complete and Partial Oxidation Catalyzed by Pt-Doped CeO2. *J. Catal.*, **2010**, *273*, 125–137.
[24] Zhang, X.; Shi, H.; Xu, B.-Q. Catalysis by Gold: Isolated Surface Au3+ Ions Are Active Sites for Selective Hydrogenation of 1,3-Butadiene over Au/ZrO2 Catalysts. *Angew. Chem. Int. Ed.*, **2005**, *44*, 7132–7135.
[25] Qiao, B.; Wang, A.; Yang, X.; Allard, L.F.; Jiang, Z.; Cui, Y.; Liu, J.; Li, J.; Zhang, T. Single-Atom Catalysis of CO Oxidation Using Pt_1/FeO_x. *Nat. Chem.*, **2011**, *3*, 634–641.
[26] Piccolo, L. Restructuring Effects of the Chemical Environment in Metal Nanocatalysis and Single-Atom Catalysis. *Catal. Today*, *in press, doi: 10.1016/j.cattod.2020.03.052*.
[27] Liu, Q.; Zhang, Z. Platinum Single-Atom Catalysts: A Comparative Review towards Effective Characterization. *Catal. Sci. Technol.*, **2019**, *9*, 4821–4834.
[28] Moses-DeBusk, M.; Yoon, M.; Allard, L.F.; Mullins, D.R.; Wu, Z.; Yang, X.; Veith, G.; Stocks, G.M.; Narula, C.K. CO Oxidation on Supported Single Pt Atoms: Experimental and Ab Initio Density Functional Studies of CO Interaction with Pt Atom on θ-Al_2O_3(010) Surface. *J. Am. Chem. Soc.*, **2013**, *135*, 12634–12645.
[29] Yang, M.; Allard, L.F.; Flytzani-Stephanopoulos, M. Atomically Dispersed Au–$(OH)_x$ Species Bound on Titania Catalyze the Low-Temperature Water-Gas Shift Reaction. *J. Am. Chem. Soc.*, **2013**, *135*, 3768–3771.
[30] Lin, J.; Wang, A.; Qiao, B.; Liu, X.; Yang, X.; Wang, X.; Liang, J.; Li, J.; Liu, J.; Zhang, T. Remarkable Performance of Ir1/FeOx Single-Atom Catalyst in Water Gas Shift Reaction. *J. Am. Chem. Soc.*, **2013**, *135*, 15314–15317.

[31] Mastikhin, V.M.; Lapina, O.B.; Balzhinimaev, B.S.; Simonova, L.G.; Karnatovskaya, L.M.; Ivanov, A.A. Catalytically Active Complexes and Influence of SiO2 on the Catalytic Properties of the Active Component of Vanadium Catalysts for SO2 Oxidation. *J. Catal.*, **1987**, *103*, 160–169.
[32] Hardcastle, F.D.; Wachs, I.E.; Horsley, J.A.; Via, G.H. The Structure of Surface Rhenium Oxide on Alumina from Laser Raman Spectroscopy and X-Ray Absorption near-Edge Spectroscopy. *J. Mol. Catal.*, **1988**, *46*, 15–36.
[33] Hardcastle, F.D.; Wachs, I.E. Raman Spectroscopy of Chromium Oxide Supported on Alumina, Titania, and Silica: A Comparative Study. In: *Olefin Metathesis and Polymerization Catalysts: Synthesis, Mechanism and Utilization*; İmamoğlu, Y.; Zümreoğlu-Karan, B.; Amass, A.J., Eds.; NATO ASI Series; Springer Netherlands: Dordrecht, **1990**; pp. 545–545.
[34] Hannagan, R.T.; Giannakakis, G.; Flytzani-Stephanopoulos, M.; Sykes, E.C.H. Single-Atom Alloy Catalysis. *Chem. Rev.*, **2020**, *120*, 12044–12088.
[35] Wei, H.; Liu, X.; Wang, A.; Zhang, L.; Qiao, B.; Yang, X.; Huang, Y.; Miao, S.; Liu, J.; Zhang, T. FeO_x-Supported Platinum Single-Atom and Pseudo-Single-Atom Catalysts for Chemoselective Hydrogenation of Functionalized Nitroarenes. *Nat. Commun.*, **2014**, *5*, 5634.
[36] Zhou, J.; Xu, Z.; Xu, M.; Zhou, X.; Wu, K. A Perspective on Oxide-Supported Single-Atom Catalysts. *Nanoscale Adv.*, **2020**, *2*, 3624–3631.
[37] Lang, R.; Du, X.; Huang, Y.; Jiang, X.; Zhang, Q.; Guo, Y.; Liu, K.; Qiao, B.; Wang, A.; Zhang, T. Single-Atom Catalysts Based on the Metal–Oxide Interaction. *Chem. Rev.*, **2020**, *120*, 11986–12043.
[38] Hemmingson, S.L.; Campbell, C.T. Trends in Adhesion Energies of Metal Nanoparticles on Oxide Surfaces: Understanding Support Effects in Catalysis and Nanotechnology. *ACS Nano*, **2017**, *11*, 1196–1203.
[39] O'Connor, N.J.; Jonayat, A.S.M.; Janik, M.J.; Senftle, T.P. Interaction Trends between Single Metal Atoms and Oxide Supports Identified with Density Functional Theory and Statistical Learning. *Nat. Catal.*, **2018**, *1*, 531–539.
[40] Dietze, E.M.; Plessow, P.N. Predicting the Strength of Metal–Support Interaction with Computational Descriptors for Adhesion Energies. *J. Phys. Chem. C*, **2019**, *123*, 20443–20450.
[41] Tan, K.; Dixit, M.; Dean, J.; Mpourmpakis, G. Predicting Metal–Support Interactions in Oxide-Supported Single-Atom Catalysts. *Ind. Eng. Chem. Res.*, **2019**, *58*, 20236–20246.
[42] Mars, P.; van Krevelen, D.W. Oxidations Carried out by Means of Vanadium Oxide Catalysts. *Chem. Eng. Sci.*, **1954**, *3*, 41–59.
[43] Langmuir, I. The Mechanism of the Catalytic Action of Platinum in the Reactions 2CO + O2 = 2CO2 and 2H2 + O2 = 2H2O. *Trans. Faraday Soc.*, **1922**, *17*, 621–654.
[44] Beniya, A.; Higashi, S. Towards Dense Single-Atom Catalysts for Future Automotive Applications. *Nat. Catal.*, **2019**, *2*, 590–602.
[45] Lambert, C.K. Current State of the Art and Future Needs for Automotive Exhaust Catalysis. *Nat. Catal.*, **2019**, *2*, 554–557.
[46] Getsoian, A. (Bean); Theis, J.R.; Paxton, W.A.; Lance, M.J.; Lambert, C.K. Remarkable Improvement in Low Temperature Performance of Model Three-Way Catalysts through Solution Atomic Layer Deposition. *Nat. Catal.*, **2019**, *2*, 614–622.
[47] Zhang, H.; Fang, S.; Hu, Y.H. Recent Advances in Single-Atom Catalysts for CO Oxidation. *Catal. Rev. Sci. Eng.*, **2020**, *in press, doi: 10.1080/01614940.2020.1821443*.

[48] Lu, Y.; Zhang, Z.; Lin, F.; Wang, H.; Wang, Y. Single-Atom Automobile Exhaust Catalysts. *ChemNanoMat*, **2020**, *6*, 1659–1682.
[49] Datye, A.K.; Votsmeier, M. Opportunities and Challenges in the Development of Advanced Materials for Emission Control Catalysts. *Nat. Mater.*, **2020**, *in press, doi: 10.1038/s41563-020-00805-3*.
[50] Doherty, F.; Wang, H.; Yang, M.; Goldsmith, B.R. Nanocluster and Single-Atom Catalysts for Thermocatalytic Conversion of CO and CO2. *Catal. Sci. Technol.*, **2020**, *10*, 5772–5791.
[51] Yates, J.T.; Duncan, T.M.; Worley, S.D.; Vaughan, R.W. Infrared Spectra of Chemisorbed CO on Rh. *J. Chem. Phys.*, **1979**, *70*, 1219–1224.
[52] Ghosh, T.K.; Nair, N.N. Rh1/γ-Al2O3 Single-Atom Catalysis of O2 Activation and CO Oxidation: Mechanism, Effects of Hydration, Oxidation State, and Cluster Size. *ChemCatChem*, **2013**, *5*, 1811–1821.
[53] Dessal, C.; Len, T.; Morfin, F.; Rousset, J.-L.; Aouine, M.; Afanasiev, P.; Piccolo, L. Dynamics of Single Pt Atoms on Alumina during CO Oxidation Monitored by Operando X-Ray and Infrared Spectroscopies. *ACS Catal.*, **2019**, *9*, 5752–5759.
[54] Dessal, C.; Sangnier, A.; Chizallet, C.; Dujardin, C.; Morfin, F.; Rousset, J.-L.; Aouine, M.; Bugnet, M.; Afanasiev, P.; Piccolo, L. Atmosphere-Dependent Stability and Mobility of Catalytic Pt Single Atoms and Clusters on γ-Al_2O_3. *Nanoscale*, **2019**, *11*, 6897–6904.
[55] Lou, Y.; Liu, J. CO Oxidation on Metal Oxide Supported Single Pt Atoms: The Role of the Support. *Ind. Eng. Chem. Res.*, **2017**, *56*, 6916–6925.
[56] Newton, M.A.; Ferri, D.; Smolentsev, G.; Marchionni, V.; Nachtegaal, M. Room-Temperature Carbon Monoxide Oxidation by Oxygen over Pt/Al_2O_3 Mediated by Reactive Platinum Carbonates. *Nat. Commun.*, **2015**, *6*, 8675.
[57] Newton, M.A.; Ferri, D.; Smolentsev, G.; Marchionni, V.; Nachtegaal, M. Kinetic Studies of the Pt Carbonate-Mediated, Room-Temperature Oxidation of Carbon Monoxide by Oxygen over Pt/Al_2O_3 Using Combined, Time-Resolved XAFS, DRIFTS, and Mass Spectrometry. *J. Am. Chem. Soc.*, **2016**, *138*, 13930–13940.
[58] Ding, K.; Gulec, A.; Johnson, A.M.; Schweitzer, N.M.; Stucky, G.D.; Marks, L.D.; Stair, P.C. Identification of Active Sites in CO Oxidation and Water-Gas Shift over Supported Pt Catalysts. *Science*, **2015**, *350*, 189–192.
[59] Li, H.; Wang, M.; Luo, L.; Zeng, J. Static Regulation and Dynamic Evolution of Single-Atom Catalysts in Thermal Catalytic Reactions. *Adv. Sci.*, **2019**, *6*, 1801471.
[60] Liu, L.; Corma, A. Evolution of Isolated Atoms and Clusters in Catalysis. *Trends Chem.*, **2020**, *2*, 383–400.
[61] Zhang, Z.; Zhu, Y.; Asakura, H.; Zhang, B.; Zhang, J.; Zhou, M.; Han, Y.; Tanaka, T.; Wang, A.; Zhang, T.; Yan, N. Thermally Stable Single Atom Pt/m-Al_2O_3 for Selective Hydrogenation and CO Oxidation. *Nat. Commun.*, **2017**, *8*, 16100.
[62] Kwak, J.H.; Hu, J.; Mei, D.; Yi, C.-W.; Kim, D.H.; Peden, C.H.F.; Allard, L.F.; Szanyi, J. Coordinatively Unsaturated Al^{3+} Centers as Binding Sites for Active Catalyst Phases of Platinum on γ-Al_2O_3. *Science*, **2009**, *325*, 1670–1673.
[63] Wang, H.; Dong, J.; Allard, L.F.; Lee, S.; Oh, S.; Wang, J.; Li, W.; Shen, M.; Yang, M. Single-Site Pt/La-Al2O3 Stabilized by Barium as an Active and Stable Catalyst in Purifying CO and C3H6 Emissions. *Appl. Catal. B*, **2019**, *244*, 327–339.
[64] Peterson, E.J.; DeLaRiva, A.T.; Lin, S.; Johnson, R.S.; Guo, H.; Miller, J.T.; Kwak, J.H.; Peden, C.H.F.; Kiefer, B.; Allard, L.F.; Ribeiro, F.H.; Datye, A.K. Low-Temperature Carbon Monoxide Oxidation Catalysed by Regenerable Atomically Dispersed Palladium on Alumina. *Nat. Commun.*, **2014**, *5*, 4885.

[65] Liang, J.-X.; Lin, J.; Yang, X.-F.; Wang, A.-Q.; Qiao, B.-T.; Liu, J.; Zhang, T.; Li, J. Theoretical and Experimental Investigations on Single-Atom Catalysis: Ir1/FeOx for CO Oxidation. *J. Phys. Chem. C*, **2014**, *118*, 21945–21951.
[66] Lin, J.; Chen, Y.; Zhou, Y.; Lin, L.; Qiao, B.; Wang, A.; Liu, J.; Wang, X.; Zhang, T. More Active Ir Subnanometer Clusters than Single-Atoms for Catalytic Oxidation of CO at Low Temperature. *AIChE J.*, **2017**, *63*, 4003–4012.
[67] Chen, W.; Ma, Y.; Li, F.; Pan, L.; Gao, W.; Xiang, Q.; Shang, W.; Song, C.; Tao, P.; Zhu, H.; Pan, X.; Deng, T.; Wu, J. Strong Electronic Interaction of Amorphous Fe2O3 Nanosheets with Single-Atom Pt toward Enhanced Carbon Monoxide Oxidation. *Adv. Funct. Mater.*, **2019**, *7*, 1904278.
[68] Bliem, R.; van der Hoeven, J.; Zavodny, A.; Gamba, O.; Pavelec, J.; de Jongh, P.E.; Schmid, M.; Diebold, U.; Parkinson, G.S. An Atomic-Scale View of CO and H2 Oxidation on a Pt/Fe3O4 Model Catalyst. *Angew. Chem. Int. Ed.*, **2015**, *54*, 13999–14002.
[69] Jakub, Z.; Hulva, J.; Ryan, P.T.P.; Duncan, D.A.; Payne, D.J.; Bliem, R.; Ulreich, M.; Hofegger, P.; Kraushofer, F.; Meier, M.; Schmid, M.; Diebold, U.; Parkinson, G.S. Adsorbate-Induced Structural Evolution Changes the Mechanism of CO Oxidation on a Rh/Fe3O4(001) Model Catalyst. *Nanoscale*, **2020**, *12*, 5866–5875.
[70] Tauster, S.J.; Fung, S.C.; Garten, R.L. Strong Metal-Support Interactions. Group 8 Noble Metals Supported on Titanium Dioxide. *J. Am. Chem. Soc.*, **1978**, *100*, 170–175.
[71] Haruta, M. Size- and Support-Dependency in the Catalysis of Gold. *Catal. Today*, **1997**, *36*, 153–166.
[72] DeRita, L.; Dai, S.; Lopez-Zepeda, K.; Pham, N.; Graham, G.W.; Pan, X.; Christopher, P. Catalyst Architecture for Stable Single Atom Dispersion Enables Site-Specific Spectroscopic and Reactivity Measurements of CO Adsorbed to Pt Atoms, Oxidized Pt Clusters, and Metallic Pt Clusters on TiO_2. *J. Am. Chem. Soc.*, **2017**, *139*, 14150–14165.
[73] Thang, H.V.; Pacchioni, G.; DeRita, L.; Christopher, P. Nature of Stable Single Atom Pt Catalysts Dispersed on Anatase TiO_2. *J. Catal.*, **2018**, *367*, 104–114.
[74] DeRita, L.; Resasco, J.; Dai, S.; Boubnov, A.; Thang, H.V.; Hoffman, A.S.; Ro, I.; Graham, G.W.; Bare, S.R.; Pacchioni, G.; Pan, X.; Christopher, P. Structural Evolution of Atomically Dispersed Pt Catalysts Dictates Reactivity. *Nat. Mater.*, **2019**, *18*, 746.
[75] Liu, P.; Zhao, Y.; Qin, R.; Gu, L.; Zhang, P.; Fu, G.; Zheng, N. A Vicinal Effect for Promoting Catalysis of Pd1/TiO2: Supports of Atomically Dispersed Catalysts Play More Roles than Simply Serving as Ligands. *Sci. Bull.*, **2018**, *63*, 675–682.
[76] Hoffman, A.S.; Fang, C.-Y.; Gates, B.C. Homogeneity of Surface Sites in Supported Single-Site Metal Catalysts: Assessment with Band Widths of Metal Carbonyl Infrared Spectra. *J. Phys. Chem. Lett.*, **2016**, *7*, 3854–3860.
[77] Hadjiivanov, K.I.; Vayssilov, G.N. Characterization of Oxide Surfaces and Zeolites by Carbon Monoxide as an IR Probe Molecule. In: *Advances in Catalysis*; Academic Press, **2002**; Vol. 47, pp. 307–511.
[78] Dessal, C.; Martínez, L.; Maheu, C.; Len, T.; Morfin, F.; Rousset, J.-L.; Puzenat, E.; Afanasiev, P.; Aouine, M.; Soler, L.; Llorca, J.; Piccolo, L. Influence of Pt Particle Size and Reaction Phase on the Photocatalytic Performances of Ultradispersed Pt/TiO_2 Catalysts for Hydrogen Evolution. *J. Catal.*, **2019**, *375*, 155–163.
[79] Liu, L.; Meira, D.M.; Arenal, R.; Concepcion, P.; Puga, A.V.; Corma, A. Determination of the Evolution of Heterogeneous Single Metal Atoms and

Nanoclusters under Reaction Conditions: Which Are the Working Catalytic Sites? *ACS Catal.*, **2019**, *9*, 10626–10639.

[80] Humphrey, N.; Bac, S.; Mallikarjun Sharada, S. Ab Initio Molecular Dynamics Reveals New Metal-Binding Sites in Atomically Dispersed Pt1/TiO2 Catalysts. *J. Phys. Chem. C*, **2020**, *124*, 24187–24195.

[81] Han, B.; Guo, Y.; Huang, Y.; Xi, W.; Xu, J.; Luo, J.; Qi, H.; Ren, Y.; Liu, X.; Qiao, B.; Zhang, T. Strong Metal–Support Interactions between Pt Single Atoms and TiO_2. *Angew. Chem. Int. Ed.*, **2020**, *132*, 11922–11927.

[82] Piccolo, L.; Afanasiev, P.; Morfin, F.; Len, T.; Dessal, C.; Rousset, J.L.; Aouine, M.; Bourgain, F.; Aguilar-Tapia, A.; Proux, O.; Chen, Y.; Soler, L.; Llorca, J. Operando X-Ray Absorption Spectroscopy Investigation of Photocatalytic Hydrogen Evolution over Ultradispersed Pt/TiO2 Catalysts. *ACS Catal.*, **2020**, *10*, 12696–12705.

[83] Lee, B.-H.; Park, S.; Kim, M.; Sinha, A.K.; Lee, S.C.; Jung, E.; Chang, W.J.; Lee, K.-S.; Kim, J.H.; Cho, S.-P.; Kim, H.; Nam, K.T.; Hyeon, T. Reversible and Cooperative Photoactivation of Single-Atom Cu/TiO_2 Photocatalysts. *Nat. Mater.*, **2019**, *18*, 620–626.

[84] Tang, Y.; Asokan, C.; Xu, M.; Graham, G.W.; Pan, X.; Christopher, P.; Li, J.; Sautet, P. Rh Single Atoms on TiO_2 Dynamically Respond to Reaction Conditions by Adapting Their Site. *Nat. Commun.*, **2019**, *10*, 4488.

[85] Hoang, S.; Guo, Y.; Binder, A.J.; Tang, W.; Wang, S.; Liu, J. (Jimmy); Tran, H.; Lu, X.; Wang, Y.; Ding, Y.; Kyriakidou, E.A.; Yang, J.; Toops, T.J.; Pauly, T.R.; Ramprasad, R.; Gao, P.-X. Activating Low-Temperature Diesel Oxidation by Single-Atom Pt on TiO_2 Nanowire Array. *Nat. Commun.*, **2020**, *11*, 1062.

[86] Shi, J.L.; Zhao, X.J.; Zhang, L.Y.; Xue, X.L.; Guo, Z.X.; Gao, Y.F.; Li, S.F. An Oxidized Magnetic Au Single Atom on Doped TiO2(110) Becomes a High Performance CO Oxidation Catalyst Due to the Charge Effect. *J. Mater. Chem. A*, **2017**, *5*, 19316–19322.

[87] Yoo, M.; Yu, Y.-S.; Ha, H.; Lee, S.; Choi, J.-S.; Oh, S.; Kang, E.; Choi, H.; An, H.; Lee, K.-S.; Park, J.Y.; Celestre, R.; Marcus, M.A.; Nowrouzi, K.; Taube, D.; Shapiro, D.A.; Jung, W.; Kim, C.; Kim, H.Y. A Tailored Oxide Interface Creates Dense Pt Single-Atom Catalysts with High Catalytic Activity. *Energy Environ. Sci.*, **2020**, *13*, 1231–1239.

[88] Agarwal, S.; Mojet, B.L.; Lefferts, L.; Datye, A.K. Chapter 2 - Ceria Nanoshapes—Structural and Catalytic Properties. In: *Catalysis by Materials with Well-Defined Structures*; Wu, Z.; Overbury, S.H., Eds.; Elsevier: Amsterdam, **2015**; pp. 31–70.

[89] Mann, A.K.P.; Wu, Z.; Overbury, S.H. Chapter 3 - The Characterization and Structure-Dependent Catalysis of Ceria with Well-Defined Facets. In: *Catalysis by Materials with Well-Defined Structures*; Wu, Z.; Overbury, S.H., Eds.; Elsevier: Amsterdam, **2015**; pp. 71–97.

[90] Montini, T.; Melchionna, M.; Monai, M.; Fornasiero, P. Fundamentals and Catalytic Applications of CeO2-Based Materials. *Chem. Rev.*, **2016**, *116*, 5987–6041.

[91] Nguyen, T.-S.; Postole, G.; Loridant, S.; Bosselet, F.; Burel, L.; Aouine, M.; Massin, L.; Morfin, F.; Gélin, P.; Piccolo, L. Ultrastable Iridium-Ceria Nanopowders Synthesized in One Step by Solution Combustion for Catalytic Hydrogen Production. *J. Mater. Chem. A*, **2014**, *2*, 19822–19832.

[92] Li, P.; Chen, X.; Li, Y.; Schwank, J.W. A Review on Oxygen Storage Capacity of CeO2-Based Materials: Influence Factors, Measurement Techniques, and Applications in Reactions Related to Catalytic Automotive Emissions Control. *Catal. Today*, **2019**, *327*, 90–115.

[93] Martin, D.; Duprez, D. Mobility of Surface Species on Oxides. 1. Isotopic Exchange of 18O2 with 16O of SiO2, Al2O3, ZrO2, MgO, CeO2, and CeO2-Al2O3. Activation by Noble Metals. Correlation with Oxide Basicity. *J. Phys. Chem.*, **1996**, *100*, 9429–9438.
[94] Paier, J.; Penschke, C.; Sauer, J. Oxygen Defects and Surface Chemistry of Ceria: Quantum Chemical Studies Compared to Experiment. *Chem. Rev.*, **2013**, *113*, 3949–3985.
[95] Ma, Y.; Gao, W.; Zhang, Z.; Zhang, S.; Tian, Z.; Liu, Y.; Ho, J.C.; Qu, Y. Regulating the Surface of Nanoceria and Its Applications in Heterogeneous Catalysis. *Surf. Sci. Rep.*, **2018**, *73*, 1–36.
[96] Lafaye, G.; Barbier, J.; Duprez, D. Impact of Cerium-Based Support Oxides in Catalytic Wet Air Oxidation: Conflicting Role of Redox and Acid–Base Properties. *Catal. Today*, **2015**, *253*, 89–98.
[97] Nguyen, T.-S.; Morfin, F.; Aouine, M.; Bosselet, F.; Rousset, J.-L.; Piccolo, L. Trends in the CO Oxidation and PROX Performances of the Platinum-Group Metals Supported on Ceria. *Catal. Today*, **2015**, *253*, 106–114.
[98] Morfin, F.; Nguyen, T.-S.; Rousset, J.-L.; Piccolo, L. Synergy between Hydrogen and Ceria in Pt-Catalyzed CO Oxidation: An Investigation on Pt–CeO_2 Catalysts Synthesized by Solution Combustion. *Appl. Catal. B*, **2016**, *197*, 2–13.
[99] Pereira-Hernández, X.I.; DeLaRiva, A.; Muravev, V.; Kunwar, D.; Xiong, H.; Sudduth, B.; Engelhard, M.; Kovarik, L.; Hensen, E.J.M.; Wang, Y.; Datye, A.K. Tuning Pt-CeO2 Interactions by High-Temperature Vapor-Phase Synthesis for Improved Reducibility of Lattice Oxygen. *Nat. Commun.*, **2019**, *10*, 1358.
[100] Ye, X.; Wang, H.; Lin, Y.; Liu, X.; Cao, L.; Gu, J.; Lu, J. Insight of the Stability and Activity of Platinum Single Atoms on Ceria. *Nano Res.*, **2019**, *12*, 1401–1409.
[101] Jones, J.; Xiong, H.; DeLaRiva, A.T.; Peterson, E.J.; Pham, H.; Challa, S.R.; Qi, G.; Oh, S.; Wiebenga, M.H.; Hernández, X.I.P.; Wang, Y.; Datye, A.K. Thermally Stable Single-Atom Platinum-on-Ceria Catalysts via Atom Trapping. *Science*, **2016**, *353*, 150–154.
[102] Yu, W.-Z.; Wang, W.-W.; Li, S.-Q.; Fu, X.-P.; Wang, X.; Wu, K.; Si, R.; Ma, C.; Jia, C.-J.; Yan, C.-H. Construction of Active Site in a Sintered Copper–Ceria Nanorod Catalyst. *J. Am. Chem. Soc.*, **2019**, *141*, 17548–17557.
[103] Jiang, D.; Wan, G.; García-Vargas, C.E.; Li, L.; Pereira-Hernández, X.I.; Wang, C.; Wang, Y. Elucidation of the Active Sites in Single-Atom Pd1/CeO2 Catalysts for Low-Temperature CO Oxidation. *ACS Catal.*, **2020**, *10*, 11356–11364.
[104] Chen, J.; Wanyan, Y.; Zeng, J.; Fang, H.; Li, Z.; Dong, Y.; Qin, R.; Wu, C.; Liu, D.; Wang, M.; Kuang, Q.; Xie, Z.; Zheng, L. Surface Engineering Protocol To Obtain an Atomically Dispersed Pt/CeO2 Catalyst with High Activity and Stability for CO Oxidation. *ACS Sustainable Chem. Eng.*, **2018**, *6*, 14054–14062.
[105] Feng, Y.; Wan, Q.; Xiong, H.; Zhou, S.; Chen, X.; Pereira Hernandez, X.I.; Wang, Y.; Lin, S.; Datye, A.K.; Guo, H. Correlating DFT Calculations with CO Oxidation Reactivity on Ga-Doped Pt/CeO2 Single-Atom Catalysts. *J. Phys. Chem. C*, **2018**, *122*, 22460–22468.
[106] Vieira, L.H.; Assaf, J.M.; Assaf, E.M. Stabilization of Atomically Dispersed Rhodium Sites on Ceria-Based Supports under Reaction Conditions Probed by in Situ Infrared Spectroscopy. *Mater. Lett.*, **2020**, *277*, 128354.
[107] Tan, W.; Alsenani, H.; Xie, S.; Cai, Y.; Xu, P.; Liu, A.; Ji, J.; Gao, F.; Dong, L.; Chukwu, E.; Yang, M.; Liu, F. Tuning Single-Atom Pt1−CeO2 Catalyst for Efficient CO and C3H6 Oxidation: Size Effect of Ceria on Pt Structural Evolution. *ChemNanoMat*, **2020**, *6*, 1797–1805.

[108] Camellone, M.F.; Fabris, S. Reaction Mechanisms for the CO Oxidation on Au/CeO2 Catalysts: Activity of Substitutional Au3+/Au+ Cations and Deactivation of Supported Au+ Adatoms. *J. Am. Chem. Soc.*, **2009**, *131*, 10473–10483.
[109] Kunwar, D.; Zhou, S.; DeLaRiva, A.; Peterson, E.J.; Xiong, H.; Pereira-Hernández, X.I.; Purdy, S.C.; ter Veen, R.; Brongersma, H.H.; Miller, J.T.; Hashiguchi, H.; Kovarik, L.; Lin, S.; Guo, H.; Wang, Y.; Datye, A.K. Stabilizing High Metal Loadings of Thermally Stable Platinum Single Atoms on an Industrial Catalyst Support. *ACS Catal.*, **2019**, *9*, 3978–3990.
[110] Bruix, A.; Lykhach, Y.; Matolínová, I.; Neitzel, A.; Skála, T.; Tsud, N.; Vorokhta, M.; Stetsovych, V.; Ševčíková, K.; Mysliveček, J.; Fiala, R.; Václavů, M.; Prince, K.C.; Bruyère, S.; Potin, V.; Illas, F.; Matolín, V.; Libuda, J.; Neyman, K.M. Maximum Noble-Metal Efficiency in Catalytic Materials: Atomically Dispersed Surface Platinum. *Angew. Chem. Int. Ed.*, **2014**, *53*, 10525–10530.
[111] Nie, L.; Mei, D.; Xiong, H.; Peng, B.; Ren, Z.; Hernandez, X.I.P.; DeLaRiva, A.; Wang, M.; Engelhard, M.H.; Kovarik, L.; Datye, A.K.; Wang, Y. Activation of Surface Lattice Oxygen in Single-Atom Pt/CeO2 for Low-Temperature CO Oxidation. *Science*, **2017**, *358*, 1419–1423.
[112] Wang, C.; Gu, X.-K.; Yan, H.; Lin, Y.; Li, J.; Liu, D.; Li, W.-X.; Lu, J. Water-Mediated Mars–Van Krevelen Mechanism for CO Oxidation on Ceria-Supported Single-Atom Pt1 Catalyst. *ACS Catal.*, **2017**, *7*, 887–891.
[113] Maurer, F.; Jelic, J.; Wang, J.; Gänzler, A.; Dolcet, P.; Wöll, C.; Wang, Y.; Studt, F.; Casapu, M.; Grunwaldt, J.-D. Tracking the Formation, Fate and Consequence for Catalytic Activity of Pt Single Sites on CeO_2. *Nat. Catal.*, **2020**, *3*, 824–833.
[114] Aleksandrov, H.A.; Neyman, K.M.; Hadjiivanov, K.I.; Vayssilov, G.N. Can the State of Platinum Species Be Unambiguously Determined by the Stretching Frequency of an Adsorbed CO Probe Molecule? *Phys. Chem. Chem. Phys.*, **2016**, *18*, 22108–22121.
[115] Resasco, J.; DeRita, L.; Dai, S.; Chada, J.P.; Xu, M.; Yan, X.; Finzel, J.; Hanukovich, S.; Hoffman, A.S.; Graham, G.W.; Bare, S.R.; Pan, X.; Christopher, P. Uniformity Is Key in Defining Structure–Function Relationships for Atomically Dispersed Metal Catalysts: The Case of Pt/CeO2. *J. Am. Chem. Soc.*, **2020**, *142*, 169–184.
[116] Jeong, H.; Shin, D.; Kim, B.-S.; Bae, J.; Shin, S.; Choe, C.; Han, J.W.; Lee, H. Controlling the Oxidation State of Pt Single Atoms for Maximizing Catalytic Activity. *Angew. Chem. Int. Ed.*, **2020**, *59*, 20691–20696.
[117] Daelman, N.; Capdevila-Cortada, M.; López, N. Dynamic Charge and Oxidation State of Pt/CeO2 Single-Atom Catalysts. *Nat. Mater.*, **2019**, *18*, 1215–1221.
[118] Alexopoulos, K.; Wang, Y.; Vlachos, D.G. First-Principles Kinetic and Spectroscopic Insights into Single-Atom Catalysis. *ACS Catal.*, **2019**, *9*, 5002–5010.
[119] Lee, J.; Ryou, Y.; Kim, J.; Chan, X.; Kim, T.J.; Kim, D.H. Influence of the Defect Concentration of Ceria on the Pt Dispersion and the CO Oxidation Activity of Pt/CeO2. *J. Phys. Chem. C*, **2018**, *122*, 4972–4983.
[120] Jiang, Z.; Jing, M.; Feng, X.; Xiong, J.; He, C.; Douthwaite, M.; Zheng, L.; Song, W.; Liu, J.; Qu, Z. Stabilizing Platinum Atoms on CeO2 Oxygen Vacancies by Metal-Support Interaction Induced Interface Distortion: Mechanism and Application. *Appl. Catal. B*, **2020**, *278*, 119304.
[121] Xie, K.; Xiao, Y.; Li, H. Activating Lattice Oxygen at Twisted Surface in Mesoporous CeO2 Single Crystal for Efficient and Durable Catalytic CO Oxidation. *Angew. Chem. Int. Ed.*
[122] Nagai, Y.; Hirabayashi, T.; Dohmae, K.; Takagi, N.; Minami, T.; Shinjoh, H.; Matsumoto, S. Sintering Inhibition Mechanism of Platinum Supported on Ceria-Based Oxide and Pt-Oxide–Support Interaction. *J .Catal.*, **2006**, *242*, 103–109.

[123] Ma, Y.; Chi, B.; Liu, W.; Cao, L.; Lin, Y.; Zhang, X.; Ye, X.; Wei, S.; Lu, J. Tailoring of the Proximity of Platinum Single Atoms on CeO2 Using Phosphorus Boosts the Hydrogenation Activity. *ACS Catal.*, **2019**, *9*, 8404–8412.
[124] Qiao, B.; Liu, J.; Wang, Y.-G.; Lin, Q.; Liu, X.; Wang, A.; Li, J.; Zhang, T.; Liu, J. (Jimmy). Highly Efficient Catalysis of Preferential Oxidation of CO in H2-Rich Stream by Gold Single-Atom Catalysts. *ACS Catal.*, **2015**, *5*, 6249–6254.
[125] Tang, Y.; Wang, Y.-G.; Li, J. Theoretical Investigations of Pt1@CeO2 Single-Atom Catalyst for CO Oxidation. *J. Phys. Chem. C*, **2017**, *121*, 11281–11289.
[126] Han, B.; Li, T.; Zhang, J.; Zeng, C.; Matsumoto, H.; Su, Y.; Qiao, B.; Zhang, T. A Highly Active Rh1/CeO2 Single-Atom Catalyst for Low-Temperature CO Oxidation. *Chem. Commun.*, **2020**, *56*, 4870–4873.
[127] Zhao, S.; Chen, F.; Duan, S.; Shao, B.; Li, T.; Tang, H.; Lin, Q.; Zhang, J.; Li, L.; Huang, J.; Bion, N.; Liu, W.; Sun, H.; Wang, A.-Q.; Haruta, M.; Qiao, B.; Li, J.; Liu, J.; Zhang, T. Remarkable Active-Site Dependent H2O Promoting Effect in CO Oxidation. *Nat. Commun.*, **2019**, *10*, 1–9.
[128] Hegde, M.S.; Bera, P. Noble Metal Ion Substituted CeO2 Catalysts: Electronic Interaction between Noble Metal Ions and CeO2 Lattice. *Catal. Today*, **2015**, *253*, 40–50.
[129] Kibis, L.S.; Kardash, T.Yu.; Derevyannikova, E.A.; Stonkus, O.A.; Slavinskaya, E.M.; Svetlichnyi, V.A.; Boronin, A.I. Redox and Catalytic Properties of RhxCe1–XO2−δ Solid Solution. *J. Phys. Chem. C*, **2017**, *121*, 26925–26938.
[130] Wang, H.; Liu, J.-X.; Allard, L.F.; Lee, S.; Liu, J.; Li, H.; Wang, J.; Wang, J.; Oh, S.H.; Li, W.; Flytzani-Stephanopoulos, M.; Shen, M.; Goldsmith, B.R.; Yang, M. Surpassing the Single-Atom Catalytic Activity Limit through Paired Pt-O-Pt Ensemble Built from Isolated Pt_1 Atoms. *Nat. Commun.*, **2019**, *10*, 1–12.
[131] Kaper, H.; Meunier, F.C.; Cardenas, L.; Šmíd, B.; Vorokhta, M.; Grosjean, R.; Aubert, D.; Dembélé, K.; Lunkenbein, T. Synergy between Metallic and Oxidized Pt Sites Unravelled during Room Temperature CO Oxidation on Pt/Ceria. *Angew. Chem. Int. Ed.*, *in press, doi: 10.1002/ange.202013223*.
[132] Guo, L.-W.; Du, P.-P.; Fu, X.-P.; Ma, C.; Zeng, J.; Si, R.; Huang, Y.-Y.; Jia, C.-J.; Zhang, Y.-W.; Yan, C.-H. Contributions of Distinct Gold Species to Catalytic Reactivity for Carbon Monoxide Oxidation. *Nat. Commun.*, **2016**, *7*, 1–8.
[133] Gänzler, A.M.; Casapu, M.; Vernoux, P.; Loridant, S.; Aires, F.J.C.S.; Epicier, T.; Betz, B.; Hoyer, R.; Grunwaldt, J.-D. Tuning the Structure of Platinum Particles on Ceria In Situ for Enhancing the Catalytic Performance of Exhaust Gas Catalysts. *Angew. Chem. Int. Ed.*, **2017**, *56*, 13078–13082.
[134] Gänzler, A.M.; Casapu, M.; Maurer, F.; Störmer, H.; Gerthsen, D.; Ferré, G.; Vernoux, P.; Bornmann, B.; Frahm, R.; Murzin, V.; Nachtegaal, M.; Votsmeier, M.; Grunwaldt, J.-D. Tuning the Pt/CeO2 Interface by in Situ Variation of the Pt Particle Size. *ACS Catal.*, **2018**, *8*, 4800–4811.
[135] Ferré, G.; Aouine, M.; Bosselet, F.; Burel, L.; Aires, F.J.C.S.; Geantet, C.; Ntais, S.; Maurer, F.; Casapu, M.; Grunwaldt, J.-D.; Epicier, T.; Loridant, S.; Vernoux, P. Exploiting the Dynamic Properties of Pt on Ceria for Low-Temperature CO Oxidation. *Catal. Sci. Technol.*, **2020**, *10*, 3904–3917.
[136] Sarma, B.B.; Plessow, P.N.; Agostini, G.; Concepción, P.; Pfänder, N.; Kang, L.; Wang, F.R.; Studt, F.; Prieto, G. Metal-Specific Reactivity in Single-Atom Catalysts: CO Oxidation on 4d and 5d Transition Metals Atomically Dispersed on MgO. *J. Am. Chem. Soc.*, **2020**, *142*, 14890–14902.
[137] Zhou, X.; Yang, W.; Chen, Q.; Geng, Z.; Shao, X.; Li, J.; Wang, Y.; Dai, D.; Chen, W.; Xu, G.; Yang, X.; Wu, K. Stable Pt Single Atoms and Nanoclusters on Ultrathin

CuO Film and Their Performances in CO Oxidation. *J. Phys. Chem. C*, **2016**, *120*, 1709–1715.
[138] Therrien, A.J.; Hensley, A.J.R.; Marcinkowski, M.D.; Zhang, R.; Lucci, F.R.; Coughlin, B.; Schilling, A.C.; McEwen, J.-S.; Sykes, E.C.H. An Atomic-Scale View of Single-Site Pt Catalysis for Low-Temperature CO Oxidation. *Nat. Catal.*, **2018**, *1*, 192–198.
[139] Zhou, X.; Shen, Q.; Yuan, K.; Yang, W.; Chen, Q.; Geng, Z.; Zhang, J.; Shao, X.; Chen, W.; Xu, G.; Yang, X.; Wu, K. Unraveling Charge State of Supported Au Single-Atoms during CO Oxidation. *J. Am. Chem. Soc.*, **2018**, *140*, 554–557.
[140] Wang, C.; Tissot, H.; Stenlid, J.H.; Kaya, S.; Weissenrieder, J. High-Density Isolated Fe1O3 Sites on a Single-Crystal Cu2O(100) Surface. *J. Phys. Chem. Lett.*, **2019**, *10*, 7318–7323.
[141] Kropp, T.; Lu, Z.; Li, Z.; Chin, Y.-H.C.; Mavrikakis, M. Anionic Single-Atom Catalysts for CO Oxidation: Support-Independent Activity at Low Temperatures. *ACS Catal.*, **2019**, *9*, 1595–1604.
[142] Lu, Y.; Wang, J.; Yu, L.; Kovarik, L.; Zhang, X.; Hoffman, A.S.; Gallo, A.; Bare, S.R.; Sokaras, D.; Kroll, T.; Dagle, V.; Xin, H.; Karim, A.M. Identification of the Active Complex for CO Oxidation over Single-Atom Ir-on-MgAl2O4 Catalysts. *Nat. Catal.*, **2019**, *2*, 149.
[143] Lou, Y.; Cai, Y.; Hu, W.; Wang, L.; Dai, Q.; Zhan, W.; Guo, Y.; Hu, P.; Cao, X.-M.; Liu, J.; Guo, Y. Identification of Active Area as Active Center for CO Oxidation over Single Au Atom Catalyst. *ACS Catal.*, **2020**, *10*, 6094–6101.
[144] Xu, Z.; Zhang, Y.; Qin, L.; Meng, Q.; Xue, Z.; Qiu, L.; Zhang, G.; Guo, X.; Li, Q. Crystal Facet Induced Single-Atom Pd/CoxOy on a Tunable Metal–Support Interface for Low Temperature Catalytic Oxidation. *Small*, **2020**, *16*, 2002071.
[145] Xu, H.; Zhang, Z.; Liu, J.; Do-Thanh, C.-L.; Chen, H.; Xu, S.; Lin, Q.; Jiao, Y.; Wang, J.; Wang, Y.; Chen, Y.; Dai, S. Entropy-Stabilized Single-Atom Pd Catalysts via High-Entropy Fluorite Oxide Supports. *Nat. Commun.*, **2020**, *11*, 3908.
[146] Wang, T.; Xing, J.-Y.; Jia, A.-P.; Tang, C.; Wang, Y.-J.; Luo, M.-F.; Lu, J.-Q. CO Oxidation over Pt/Cr1.3Fe0.7O3 Catalysts: Enhanced Activity on Single Pt Atom by H2O Promotion. *J. Catal.*, **2020**, *382*, 192–203.
[147] Lu, Y.; Kuo, C.-T.; Kovarik, L.; Hoffman, A.S.; Boubnov, A.; Driscoll, D.M.; Morris, J.R.; Bare, S.R.; Karim, A.M. A Versatile Approach for Quantification of Surface Site Fractions Using Reaction Kinetics: The Case of CO Oxidation on Supported Ir Single Atoms and Nanoparticles. *J. Catal.*, **2019**, *378*, 121–130.
[148] Resasco, J.; Yang, F.; Mou, T.; Wang, B.; Christopher, P.; Resasco, D.E. Relationship between Atomic Scale Structure and Reactivity of Pt Catalysts: Hydrodeoxygenation of m-Cresol over Isolated Pt Cations and Clusters. *ACS Catal.*, **2020**, *10*, 595–603.
[149] Xu, H.; Xu, C.-Q.; Cheng, D.; Li, J. Identification of Activity Trends for CO Oxidation on Supported Transition-Metal Single-Atom Catalysts. *Catal. Sci. Technol.*, **2017**, *7*, 5860–5871.
[150] Qiao, B.; Liu, J.; Wang, Y.-G.; Lin, Q.; Liu, X.; Wang, A.; Li, J.; Zhang, T.; Liu, J. (Jimmy). Highly Efficient Catalysis of Preferential Oxidation of CO in H2-Rich Stream by Gold Single-Atom Catalysts. *ACS Catal.*, **2015**, *5*, 6249–6254.
[151] Gan, T.; He, Q.; Zhang, H.; Xiao, H.; Liu, Y.; Zhang, Y.; He, X.; Ji, H. Unveiling the Kilogram-Scale Gold Single-Atom Catalysts via Ball Milling for Preferential Oxidation of CO in Excess Hydrogen. *Chem. Eng. J.*, **2020**, *389*, 124490.
[152] Lin, J.; Qiao, B.; Liu, J.; Huang, Y.; Wang, A.; Li, L.; Zhang, W.; Allard, L.F.; Wang, X.; Zhang, T. Design of a Highly Active Ir/Fe(OH)x Catalyst: Versatile Application

of Pt-Group Metals for the Preferential Oxidation of Carbon Monoxide. *Angew. Chem. Int. Ed.*, **2012**, *51*, 2920–2924.
[153] Guan, H.; Lin, J.; Li, L.; Wang, X.; Zhang, T. Highly Active Subnano Rh/Fe(OH)x Catalyst for Preferential Oxidation of CO in H2-Rich Stream. *Appl. Catal. B*, **2016**, *184*, 299–308.
[154] Cao, L.; Liu, W.; Luo, Q.; Yin, R.; Wang, B.; Weissenrieder, J.; Soldemo, M.; Yan, H.; Lin, Y.; Sun, Z.; Ma, C.; Zhang, W.; Chen, S.; Wang, H.; Guan, Q.; Yao, T.; Wei, S.; Yang, J.; Lu, J. Atomically Dispersed Iron Hydroxide Anchored on Pt for Preferential Oxidation of CO in H2. *Nature*, **2019**, *565*, 631.
[155] Zhang, H.; Liu, X.; Zhang, N.; Zheng, J.; Zheng, Y.; Li, Y.; Zhong, C.-J.; Chen, B.H. Construction of Ultrafine and Stable PtFe Nano-Alloy with Ultra-Low Pt Loading for Complete Removal of CO in PROX at Room Temperature. *Appl. Catal. B*, **2016**, *180*, 237–245.
[156] Cao, S.; Zhao, Y.; Lee, S.; Yang, S.; Liu, J.; Giannakakis, G.; Li, M.; Ouyang, M.; Wang, D.; Sykes, E.C.H.; Flytzani-Stephanopoulos, M. High-Loading Single Pt Atom Sites [Pt-O(OH)x] Catalyze the CO PROX Reaction with High Activity and Selectivity at Mild Conditions. *Sci. Adv.*, **2020**, *6*, eaba3809.
[157] Quinet, E.; Piccolo, L.; Morfin, F.; Avenier, P.; Diehl, F.; Caps, V.; Rousset, J.L. On the Mechanism of Hydrogen-Promoted Gold-Catalyzed CO Oxidation. *J. Catal.*, **2009**, *268*, 384–389.
[158] Pal, D.B.; Chand, R.; Upadhyay, S.N.; Mishra, P.K. Performance of Water Gas Shift Reaction Catalysts: A Review. *Renewable Sustainable Energy Rev.*, **2018**, *93*, 549–565.
[159] Saeidi, S.; Fazlollahi, F.; Najari, S.; Iranshahi, D.; Klemeš, J.J.; Baxter, L.L. Hydrogen Production: Perspectives, Separation with Special Emphasis on Kinetics of WGS Reaction: A State-of-the-Art Review. *J. Ind. Eng. Chem.*, **2017**, *49*, 1–25.
[160] Zhu, M.; Wachs, I.E. Iron-Based Catalysts for the High-Temperature Water–Gas Shift (HT-WGS) Reaction: A Review. *ACS Catal.*, **2016**, *6*, 722–732.
[161] Gradisher, L.; Dutcher, B.; Fan, M. Catalytic Hydrogen Production from Fossil Fuels via the Water Gas Shift Reaction. *Applied Energy*, **2015**, *139*, 335–349.
[162] Haruta, M. Spiers Memorial Lecture. *Faraday Discuss.*, **2011**, *152*, 11–32.
[163] Sakurai, H.; Akita, T.; Tsubota, S.; Kiuchi, M.; Haruta, M. Low-Temperature Activity of Au/CeO2 for Water Gas Shift Reaction, and Characterization by ADF-STEM, Temperature-Programmed Reaction, and Pulse Reaction. *Appl. Catal. A*, **2005**, *291*, 179–187.
[164] Oyama, S.T.; Gaudet, J.; Zhang, W.; Su, D.S.; Bando, K.K. Platinum-Like Catalytic Behavior of Au+. *ChemCatChem*, **2010**, *2*, 1582–1586.
[165] Gaudet, J.; Bando, K.K.; Song, Z.; Fujitani, T.; Zhang, W.; Su, D.S.; Oyama, S.T. Effect of Gold Oxidation State on the Epoxidation and Hydrogenation of Propylene on Au/TS-1. *J. Catal.*, **2011**, *280*, 40–49.
[166] Zhai, Y.; Pierre, D.; Si, R.; Deng, W.; Ferrin, P.; Nilekar, A.U.; Peng, G.; Herron, J.A.; Bell, D.C.; Saltsburg, H.; Mavrikakis, M.; Flytzani-Stephanopoulos, M. Alkali-Stabilized Pt-OHx Species Catalyze Low-Temperature Water-Gas Shift Reactions. *Science*, **2010**, *329*, 1633–1636.
[167] Yang, M.; Allard, L.F.; Flytzani-Stephanopoulos, M. Atomically Dispersed Au–(OH)x Species Bound on Titania Catalyze the Low-Temperature Water-Gas Shift Reaction. *J. Am. Chem. Soc.*, **2013**, *135*, 3768–3771.
[168] Flytzani-Stephanopoulos, M. Gold Atoms Stabilized on Various Supports Catalyze the Water–Gas Shift Reaction. *Acc. Chem. Res.*, **2014**, *47*, 783–792.

[169] Yang, M.; Li, S.; Wang, Y.; Herron, J.A.; Xu, Y.; Allard, L.F.; Lee, S.; Huang, J.; Mavrikakis, M.; Flytzani-Stephanopoulos, M. Catalytically Active Au-O(OH)x-Species Stabilized by Alkali Ions on Zeolites and Mesoporous Oxides. *Science*, **2014**, *346*, 1498–1501.
[170] Yang, M.; Liu, J.; Lee, S.; Zugic, B.; Huang, J.; Allard, L.F.; Flytzani-Stephanopoulos, M. A Common Single-Site Pt(II)–O(OH)x– Species Stabilized by Sodium on "Active" and "Inert" Supports Catalyzes the Water-Gas Shift Reaction. *J. Am. Chem. Soc.*, **2015**, *137*, 3470–3473.
[171] Ammal, S.C.; Heyden, A. Understanding the Nature and Activity of Supported Platinum Catalysts for the Water–Gas Shift Reaction: From Metallic Nanoclusters to Alkali-Stabilized Single-Atom Cations. *ACS Catal.*, **2019**, *9*, 7721–7740.
[172] Ding, K.; Gulec, A.; Johnson, A.M.; Schweitzer, N.M.; Stucky, G.D.; Marks, L.D.; Stair, P.C. Identification of Active Sites in CO Oxidation and Water-Gas Shift over Supported Pt Catalysts. *Science*, **2015**, *350*, 189–192.
[173] Wang, C.; Yang, M.; Flytzani-Stephanopoulos, M. Single Gold Atoms Stabilized on Nanoscale Metal Oxide Supports Are Catalytic Active Centers for Various Reactions. *AIChE J.*, **2016**, *62*, 429–439.
[174] Kuai, L.; Liu, S.; Cao, S.; Ren, Y.; Kan, E.; Zhao, Y.; Yu, N.; Li, F.; Li, X.; Wu, Z.; Wang, X.; Geng, B. Atomically Dispersed Pt/Metal Oxide Mesoporous Catalysts from Synchronous Pyrolysis–Deposition Route for Water–Gas Shift Reaction. *Chem. Mater.*, **2018**, *30*, 5534–5538.
[175] Yang, M.; Flytzani-Stephanopoulos, M. Design of Single-Atom Metal Catalysts on Various Supports for the Low-Temperature Water-Gas Shift Reaction. *Catal. Today*, **2017**, *298*, 216–225.
[176] Yi, N.; Si, R.; Saltsburg, H.; Flytzani-Stephanopoulos, M. Active Gold Species on Cerium Oxide Nanoshapes for Methanol Steam Reforming and the Water Gas Shift Reactions. *Energy Environ. Sci.*, **2010**, *3*, 831–837.
[177] Xiang, Y.; He, J.; Sun, N.; Fan, Y.; Yang, L.; Fang, C.; Kuai, L. Hollow Mesoporous CeO2 Microspheres for Efficient Loading of Au Single-Atoms to Catalyze the Water-Gas Shift Reaction. *Microp. Mesop. Mater.*, **2020**, *308*, 110507.
[178] Guan, H.; Lin, J.; Qiao, B.; Miao, S.; Wang, A.-Q.; Wang, X.; Zhang, T. Enhanced Performance of Rh1/TiO2 Catalyst without Methanation in Water-Gas Shift Reaction. *AIChE J.*, **2017**, *63*, 2081–2088.
[179] Lin, J.; Wang, A.; Qiao, B.; Liu, X.; Yang, X.; Wang, X.; Liang, J.; Li, J.; Liu, J.; Zhang, T. Remarkable Performance of Ir1/FeOx Single-Atom Catalyst in Water Gas Shift Reaction. *J. Am. Chem. Soc.*, **2013**, *135*, 15314–15317.
[180] Sun, X.; Lin, J.; Zhou, Y.; Li, L.; Su, Y.; Wang, X.; Zhang, T. FeOx Supported Single-Atom Pd Bifunctional Catalyst for Water Gas Shift Reaction. *AIChE Journal*, **2017**, *63*, 4022–4031.
[181] Gai, P.L.; Yoshida, K.; Ward, M.R.; Walsh, M.; Baker, R.T.; Water, L. van de; Watson, M.J.; Boyes, E.D. Visualisation of Single Atom Dynamics in Water Gas Shift Reaction for Hydrogen Generation. *Catal. Sci. Technol.*, **2016**, *6*, 2214–2227.
[182] Nelson, N.C.; Chen, L.; Meira, D.; Kovarik, L.; Szanyi, J. In Situ Dispersion of Palladium on TiO2 During Reverse Water–Gas Shift Reaction: Formation of Atomically Dispersed Palladium. *Angew. Chem. Int. Ed.*, **2020**, *59*, 17657–17663.
[183] Chen, Y.; Lin, J.; Li, L.; Qiao, B.; Liu, J.; Su, Y.; Wang, X. Identifying Size Effects of Pt as Single Atoms and Nanoparticles Supported on FeOx for the Water-Gas Shift Reaction. *ACS Catal.*, **2018**, *8*, 859–868.

[184] Liang, J.-X.; Lin, J.; Liu, J.; Wang, X.; Zhang, T.; Li, J. Dual Metal Active Sites in an Ir1/FeOx Single-Atom Catalyst: A Redox Mechanism for the Water-Gas Shift Reaction. *Angew. Chem. Int. Ed.*, **2020**, *59*, 12868–12875.
[185] Yan, D.; Chen, J.; Jia, H. Temperature-Induced Structure Reconstruction to Prepare a Thermally Stable Single-Atom Platinum Catalyst. *Angew. Chem. Int. Ed.*, **2020**, *59*, 13562–13567.
[186] Duan, Q.; Zhang, C.; Sun, S.; Pan, Y.; Zhou, X.; Liu, Y.; Chen, K.; Li, C.; Wang, X.; Li, W. Atomically Dispersed Palladium-Based Catalysts Obtained via Constructing a Spatial Structure with High Performance for Lean Methane Combustion. *J. Mater. Chem. A*, **2020**, *8*, 7395–7404.
[187] Huang, Z.; Gu, X.; Cao, Q.; Hu, P.; Hao, J.; Li, J.; Tang, X. Catalytically Active Single-Atom Sites Fabricated from Silver Particles. *Angew. Chem. Int. Ed.*, **2012**, *51*, 4198–4203.
[188] Chen, Y.; Huang, Z.; Zhou, M.; Ma, Z.; Chen, J.; Tang, X. Single Silver Adatoms on Nanostructured Manganese Oxide Surfaces: Boosting Oxygen Activation for Benzene Abatement. *Environ. Sci. Technol.*, **2017**, *51*, 2304–2311.
[189] Chen, Y.; Gao, J.; Huang, Z.; Zhou, M.; Chen, J.; Li, C.; Ma, Z.; Chen, J.; Tang, X. Sodium Rivals Silver as Single-Atom Active Centers for Catalyzing Abatement of Formaldehyde. *Environ. Sci. Technol.*, **2017**, *51*, 7084–7090.
[190] Zhang, C.; Liu, F.; Zhai, Y.; Ariga, H.; Yi, N.; Liu, Y.; Asakura, K.; Flytzani-Stephanopoulos, M.; He, H. Alkali-Metal-Promoted Pt/TiO2 Opens a More Efficient Pathway to Formaldehyde Oxidation at Ambient Temperatures. *Angew. Chem. Int. Ed.*, **2012**, *51*, 9628–9632.
[191] Liu, T.; Li, Q.; Xin, Y.; Zhang, Z.; Tang, X.; Zheng, L.; Gao, P.-X. Quasi Free K Cations Confined in Hollandite-Type Tunnels for Catalytic Solid (Catalyst)-Solid (Reactant) Oxidation Reactions. *Appl. Catal. B*, **2018**, *232*, 108–116.
[192] Zhang, H.; Sui, S.; Zheng, X.; Cao, R.; Zhang, P. One-Pot Synthesis of Atomically Dispersed Pt on MnO2 for Efficient Catalytic Decomposition of Toluene at Low Temperatures. *Appl. Catal. B*, **2019**, *257*, 117878.
[193] Xu, L.; Chen, D.; Qu, J.; Wang, L.; Tang, J.; Liu, H.; Yang, J. Replacement Reaction-Based Synthesis of Supported Palladium Catalysts with Atomic Dispersion for Catalytic Removal of Benzene. *J. Mater. Chem. A*, **2018**, *6*, 17032–17039.
[194] Yang, K.; Liu, Y.; Deng, J.; Zhao, X.; Yang, J.; Han, Z.; Hou, Z.; Dai, H. Three-Dimensionally Ordered Mesoporous Iron Oxide-Supported Single-Atom Platinum: Highly Active Catalysts for Benzene Combustion. *Appl. Catal. B*, **2019**, *244*, 650–659.
[195] Jiang, Z.; Feng, X.; Deng, J.; He, C.; Douthwaite, M.; Yu, Y.; Liu, J.; Hao, Z.; Zhao, Z. Atomic-Scale Insights into the Low-Temperature Oxidation of Methanol over a Single-Atom Pt1-Co3O4 Catalyst. *Adv. Funct. Mater.*, **2019**, *29*, 1902041.
[196] Zhang, Q.; Qin, X.-X.; Duan-Mu, F.-P.; Ji, H.-M.; Shen, Z.-R.; Han, X.-P.; Hu, W.-B. Isolated Platinum Atoms Stabilized by Amorphous Tungstenic Acid: Metal–Support Interaction for Synergistic Oxygen Activation. *Angew. Chem. Int. Ed.*, **2018**, *57*, 9351–9356.
[197] Grasselli, R.K. Genesis of Site Isolation and Phase Cooperation in Selective Oxidation Catalysis. *Top. Catal.*, **2001**, *15*, 93–101.
[198] Grasselli, R.K. Fundamental Principles of Selective Heterogeneous Oxidation Catalysis. *Top. Catal.*, **2002**, *21*, 79–88.
[199] Grasselli, R.K. Site Isolation and Phase Cooperation: Two Important Concepts in Selective Oxidation Catalysis: A Retrospective. *Catal. Today*, **2014**, *238*, 10–27.

[200] Nguyen, L.D.; Loridant, S.; Launay, H.; Pigamo, A.; Dubois, J.L.; Millet, J.M.M. Study of New Catalysts Based on Vanadium Oxide Supported on Mesoporous Silica for the Partial Oxidation of Methane to Formaldehyde: Catalytic Properties and Reaction Mechanism. *J. Catal.*, **2006**, *237*, 38–48.
[201] Shannon, I.J.; Maschmeyer, T.; Oldroyd, R.D.; Sankar, G.; Thomas, J.M.; Pernot, H.; Balikdjian, J.-P.; Che, M. Metallocene-Derived, Isolated MoVI Active Centres on Mesoporous Silica for the Catalytic Dehydrogenation of Methanol. *J. Chem. Soc., Faraday Trans.*, **1998**, *94*, 1495–1499.
[202] Bradley, C.A.; McMurdo, M.J.; Tilley, T.D. Selective Catalytic Cyclohexene Oxidation Using Titanium-Functionalized Silicone Nanospheres. *J. Phys. Chem. C*, **2007**, *111*, 17570–17579.
[203] Jarupatrakorn, J.; Tilley, T.D. Silica-Supported, Single-Site Titanium Catalysts for Olefin Epoxidation. A Molecular Precursor Strategy for Control of Catalyst Structure. *J. Am. Chem. Soc.*, **2002**, *124*, 8380–8388.
[204] Ruddy, D.A.; Ohler, N.L.; Bell, A.T.; Tilley, T.D. Thermolytic Molecular Precursor Route to Site-Isolated Vanadia–Silica Materials and Their Catalytic Performance in Methane Selective Oxidation. *J. Catal.*, **2006**, *238*, 277–285.
[205] Lee, C.-H.; Lin, T.-S.; Mou, C.-Y. (VO)2+ Ions Immobilized on Functionalized Surface of Mesoporous Silica and Their Activity toward the Hydroxylation of Benzene. *J. Phys. Chem. B*, **2003**, *107*, 2543–2551.
[206] Rossetti, I.; Mancini, G.F.; Ghigna, P.; Scavini, M.; Piumetti, M.; Bonelli, B.; Cavani, F.; Comite, A. Spectroscopic Enlightening of the Local Structure Of VOX Active Sites in Catalysts for the Odh of Propane. *J. Phys. Chem. C*, **2012**, *116*, 22386–22398.
[207] Thomas, J.M. How Far Is the Concept of Isolated Active Sites Valid in Solid Catalysts? *Top Catal*, **2008**, *50*, 98–105.
[208] Wang, G.; Zhang, S.; Huang, Y.; Kang, F.; Yang, Z.; Guo, Y. Styrene Epoxidation over V-SBA-15 with Alkaline-Earth Metal Ion Promotion under Photo-Assisted Conditions. *Appl. Catal. A*, **2012**, *413–414*, 52–61.
[209] Du, G.; Lim, S.; Yang, Y.; Wang, C.; Pfefferle, L.; Haller, G.L. Catalytic Performance of Vanadium Incorporated MCM-41 Catalysts for the Partial Oxidation of Methane to Formaldehyde. *Appl. Catal. A*, **2006**, *302*, 48–61.
[210] Hu, Y.; Nagai, Y.; Rahmawaty, D.; Wei, C.; Anpo, M. Characteristics of the Photocatalytic Oxidation of Methane into Methanol on V-Containing MCM-41 Catalysts. *Catal. Lett.*, **2008**, *124*, 80.
[211] Chalupka, K.; Thomas, C.; Millot, Y.; Averseng, F.; Dzwigaj, S. Mononuclear Pseudo-Tetrahedral V Species of VSiBEA Zeolite as the Active Sites of the Selective Oxidative Dehydrogenation of Propane. *J. Catal.*, **2013**, *305*, 46–55.
[212] Liu, J.; Mohamed, F.; Sauer, J. Selective Oxidation of Propene by Vanadium Oxide Monomers Supported on Silica. *J. Catal.*, **2014**, *317*, 75–82.
[213] Rozanska, X.; Fortrie, R.; Sauer, J. Oxidative Dehydrogenation of Propane by Monomeric Vanadium Oxide Sites on Silica Support. *J. Phys. Chem. C*, **2007**, *111*, 6041–6050.
[214] Launay, H.; Loridant, S.; Pigamo, A.; Dubois, J.L.; Millet, J.M.M. Vanadium Species in New Catalysts for the Selective Oxidation of Methane to Formaldehyde: Specificity and Molecular Structure Dynamics with Water. *J. Catal.*, **2007**, *246*, 390–398.
[215] Launay, H.; Loridant, S.; Nguyen, D.L.; Volodin, A.M.; Dubois, J.L.; Millet, J.M.M. Vanadium Species in New Catalysts for the Selective Oxidation of Methane to Formaldehyde: Activation of the Catalytic Sites. *Catal. Today*, **2007**, *128*, 176–182.

[216] Nozaki, C.; Lugmair, C.G.; Bell, A.T.; Tilley, T.D. Synthesis, Characterization, and Catalytic Performance of Single-Site Iron(III) Centers on the Surface of SBA-15 Silica. *J. Am. Chem. Soc.*, **2002**, *124*, 13194–13203.
[217] Su, W.; Wang, S.; Ying, P.; Feng, Z.; Li, C. A Molecular Insight into Propylene Epoxidation on Cu/SiO2 Catalysts Using O2 as Oxidant. *J. Catal.*, **2009**, *268*, 165–174.
[218] Wachs, I.E. In Situ Raman Spectroscopy Studies of Catalysts. *Top. Catal.*, **1999**, *8*, 57–63.
[219] Khaliullin, R.Z.; Bell, A.T. A Density Functional Theory Study of the Oxidation of Methanol to Formaldehyde over Vanadia Supported on Silica, Titania, and Zirconia. *J. Phys. Chem. B*, **2002**, *106*, 7832–7838.
[220] Gao, X.; Jehng, J.-M.; Wachs, I.E. In Situ UV–Vis–NIR Diffuse Reflectance and Raman Spectroscopic Studies of Propane Oxidation over ZrO2-Supported Vanadium Oxide Catalysts. *J. Catal.*, **2002**, *209*, 43–50.
[221] Zhou, W.; Ross-Medgaarden, E.I.; Knowles, W.V.; Wong, M.S.; Wachs, I.E.; Kiely, C.J. Identification of Active Zr–WOx Clusters on a ZrO2 Support for Solid Acid Catalysts. *Nat. Chem.*, **2009**, *1*, 722–728.
[222] Kim, T.; Burrows, A.; Kiely, C.J.; Wachs, I.E. Molecular/Electronic Structure–Surface Acidity Relationships of Model-Supported Tungsten Oxide Catalysts. *J. Catal.*, **2007**, *246*, 370–381.
[223] Ross-Medgaarden, E.I.; Knowles, W.V.; Kim, T.; Wong, M.S.; Zhou, W.; Kiely, C.J.; Wachs, I.E. New Insights into the Nature of the Acidic Catalytic Active Sites Present in ZrO2-Supported Tungsten Oxide Catalysts. *J. Catal.*, **2008**, *256*, 108–125.
[224] Ross-Medgaarden, E.I.; Wachs, I.E.; Knowles, W.V.; Burrows, A.; Kiely, C.J.; Wong, M.S. Tuning the Electronic and Molecular Structures of Catalytic Active Sites with Titania Nanoligands. *J. Am. Chem. Soc.*, **2009**, *131*, 680–687.
[225] Figueras, F.; Palomeque, J.; Loridant, S.; Fèche, C.; Essayem, N.; Gelbard, G. Influence of the Coordination on the Catalytic Properties of Supported W Catalysts. *J. Catal.*, **2004**, *226*, 25–31.
[226] Kourieh, R.; Bennici, S.; Auroux, A. Acid and Redox Properties of Tungstated Zirconia Catalysts. *React. Kinet., Mech. Catal.*, **2012**, *105*, 101–111.
[227] Shen, Q.; Cao, C.; Huang, R.; Zhu, L.; Zhou, X.; Zhang, Q.; Gu, L.; Song, W. Single Chromium Atoms Supported on Titanium Dioxide Nanoparticles for Synergic Catalytic Methane Conversion under Mild Conditions. *Angew. Chem. Int. Ed.*, **2020**, *59*, 1216–1219.
[228] Huang, W.; Zhang, S.; Tang, Y.; Li, Y.; Nguyen, L.; Li, Y.; Shan, J.; Xiao, D.; Gagne, R.; Frenkel, A.I.; Tao, F. (Feng). Low-Temperature Transformation of Methane to Methanol on Pd1O4 Single Sites Anchored on the Internal Surface of Microporous Silicate. *Angew. Chem. Int. Ed.*, **2016**, *55*, 13441–13445.
[229] Kwon, Y.; Kim, T.Y.; Kwon, G.; Yi, J.; Lee, H. Selective Activation of Methane on Single-Atom Catalyst of Rhodium Dispersed on Zirconia for Direct Conversion. *J. Am. Chem. Soc.*, **2017**, *139*, 17694–17699.
[230] Shan, J.; Li, M.; Allard, L.F.; Lee, S.; Flytzani-Stephanopoulos, M. Mild Oxidation of Methane to Methanol or Acetic Acid on Supported Isolated Rhodium Catalysts. *Nature*, **2017**, *551*, 605–608.
[231] Bai, S.; Liu, F.; Huang, B.; Li, F.; Lin, H.; Wu, T.; Sun, M.; Wu, J.; Shao, Q.; Xu, Y.; Huang, X. High-Efficiency Direct Methane Conversion to Oxygenates on a Cerium Dioxide Nanowires Supported Rhodium Single-Atom Catalyst. *Nat. Commun.*, **2020**, *11*, 954.

[232] Zhao, Q.; Liu, B.; Xu, Y.; Jiang, F.; Liu, X. Insight into the Active Site and Reaction Mechanism for Selective Oxidation of Methane to Methanol Using H2O2 on a Rh1/ZrO2 Catalyst. *New J. Chem.*, **2020**, *44*, 1632–1639.
[233] Harrath, K.; Yu, X.; Xiao, H.; Li, J. The Key Role of Support Surface Hydrogenation in the CH4 to CH3OH Selective Oxidation by a ZrO2-Supported Single-Atom Catalyst. *ACS Catal.*, **2019**, *9*, 8903–8909.
[234] J. Bunting, R.; Thompson, J.; Hu, P. The Mechanism and Ligand Effects of Single Atom Rhodium Supported on ZSM-5 for the Selective Oxidation of Methane to Methanol. *Phys. Chem. Chem. Phys.*, **2020**, *22*, 11686–11694.
[235] Li, T.; Liu, F.; Tang, Y.; Li, L.; Miao, S.; Su, Y.; Zhang, J.; Huang, J.; Sun, H.; Haruta, M.; Wang, A.; Qiao, B.; Li, J.; Zhang, T. Maximizing the Number of Interfacial Sites in Single-Atom Catalysts for the Highly Selective, Solvent-Free Oxidation of Primary Alcohols. *Angew. Chem. Int. Ed.*, **2018**, *57*, 7795–7799.
[236] Thomas, A.; He, Q.; Edwards, J.K. Preparation of Ultra Low Loaded Au Catalysts for Oxidation Reactions. *Faraday Discuss.*, **2011**, *152*, 381–392.
[237] Cao, S.; Yang, M.; Elnabawy, A.O.; Trimpalis, A.; Li, S.; Wang, C.; Göltl, F.; Chen, Z.; Liu, J.; Shan, J.; Li, M.; Haas, T.; Chapman, K.W.; Lee, S.; Allard, L.F.; Mavrikakis, M.; Flytzani-Stephanopoulos, M. Single-Atom Gold Oxo-Clusters Prepared in Alkaline Solutions Catalyse the Heterogeneous Methanol Self-Coupling Reactions. *Nat. Chem.*, **2019**, *11*, 1098–1105.
[238] Shan, J.; Giannakakis, G.; Liu, J.; Cao, S.; Ouyang, M.; Li, M.; Lee, S.; Flytzani-Stephanopoulos, M. PdCu Single Atom Alloys for the Selective Oxidation of Methanol to Methyl Formate at Low Temperatures. *Top. Catal.*, **2020**, *63*, 618–627.
[239] Liu, L.; Corma, A. Metal Catalysts for Heterogeneous Catalysis: From Single Atoms to Nanoclusters and Nanoparticles. *Chem. Rev.*, **2018**, *118*, 4981–5079.
[240] Shang, Q.; Tang, N.; Qi, H.; Chen, S.; Xu, G.; Wu, C.; Pan, X.; Wang, X.; Cong, Y. A Palladium Single-Atom Catalyst toward Efficient Activation of Molecular Oxygen for Cinnamyl Alcohol Oxidation. *Chin. J. Catal.*, **2020**, *41*, 1812–1817.
[241] Hikazudani, S.; Mochida, T.; Yano, K.; Nagaoka, K.; Ishihara, T.; Takita, Y. Mono-Atomically Dispersed Pd on TiO2 as a Catalyst for Epoxidation of Light Olefins at Low Temperatures in the Presence of H2 and O2. *Catal. Commun.*, **2011**, *12*, 1396–1400.
[242] Liu, Y.; Gan, T.; He, Q.; Zhang, H.; He, X.; Ji, H. Catalytic Oxidation of 5-Hydroxymethylfurfural to 2,5-Diformylfuran over Atomically Dispersed Ruthenium Catalysts. *Ind. Eng. Chem. Res.*, **2020**, *59*, 4333–4337.
[243] Tang, Y.; Li, Y.; Fung, V.; Jiang, D.; Huang, W.; Zhang, S.; Iwasawa, Y.; Sakata, T.; Nguyen, L.; Zhang, X.; Frenkel, A.I.; Tao, F. (Feng). Single Rhodium Atoms Anchored in Micropores for Efficient Transformation of Methane under Mild Conditions. *Nat. Commun.*, **2018**, *9*, 1231.
[244] He, W.-L.; Yang, X.-L.; Zhao, M.; Wu, C.-D. Suspending Ionic Single-Atom Catalysts in Porphyrinic Frameworks for Highly Efficient Aerobic Oxidation at Room Temperature. *J. Catal.*, **2018**, *358*, 43–49.
[245] Babucci, M.; Guntida, A.; Gates, B.C. Atomically Dispersed Metals on Well-Defined Supports Including Zeolites and Metal–Organic Frameworks: Structure, Bonding, Reactivity, and Catalysis. *Chem. Rev.*, **2020**, *120*, 11956–11985.
[246] Chen, Z.; Liu, C.; Liu, J.; Li, J.; Xi, S.; Chi, X.; Xu, H.; Park, I.-H.; Peng, X.; Li, X.; Yu, W.; Liu, X.; Zhong, L.; Leng, K.; Huang, W.; Koh, M.J.; Loh, K.P. Cobalt Single-Atom-Intercalated Molybdenum Disulfide for Sulfide Oxidation with Exceptional Chemoselectivity. *Adv. Mater.*, **2019**, *32*, 1906437.

[247] Gawande, M.B.; Fornasiero, P.; Zbořil, R. Carbon-Based Single-Atom Catalysts for Advanced Applications. *ACS Catal.*, **2020**, *10*, 2231–2259.
[248] Li, M.; Wu, S.; Yang, X.; Hu, J.; Peng, L.; Bai, L.; Huo, Q.; Guan, J. Highly Efficient Single Atom Cobalt Catalyst for Selective Oxidation of Alcohols. *Appl. Catal. A*, **2017**, *543*, 61–66.
[249] Xie, J.; Yin, K.; Serov, A.; Artyushkova, K.; Pham, H.N.; Sang, X.; Unocic, R.R.; Atanassov, P.; Datye, A.K.; Davis, R.J. Selective Aerobic Oxidation of Alcohols over Atomically-Dispersed Non-Precious Metal Catalysts. *ChemSusChem*, **2017**, *10*, 359–362.
[250] Ding, Y.; Zhang, P.; Xiong, H.; Sun, X.; Klyushin, A.; Zhang, B.; Liu, Z.; Zhang, J.; Zhu, H.; Qiao, Z.-A.; Heumann, S.; Dai, S. Tuning Regioselective Oxidation toward Phenol via Atomically Dispersed Iron Sites on Carbon. *Green Chem.*, **2020**, *22*, 6025–6032.
[251] Liu, W.; Zhang, L.; Liu, X.; Liu, X.; Yang, X.; Miao, S.; Wang, W.; Wang, A.; Zhang, T. Discriminating Catalytically Active FeNx Species of Atomically Dispersed Fe–N–C Catalyst for Selective Oxidation of the C–H Bond. *J. Am. Chem. Soc.*, **2017**, *139*, 10790–10798.
[252] Bakandritsos, A.; Kadam, R.G.; Kumar, P.; Zoppellaro, G.; Medved', M.; Tuček, J.; Montini, T.; Tomanec, O.; Andrýsková, P.; Drahoš, B.; Varma, R.S.; Otyepka, M.; Gawande, M.B.; Fornasiero, P.; Zbořil, R. Mixed-Valence Single-Atom Catalyst Derived from Functionalized Graphene. *Adv. Mater.*, **2019**, *31*, 1900323.
[253] Huang, G.; Wang, L.; Luo, H.; Shang, S.; Chen, B.; Gao, S.; An, Y. Isopropanol as a Hydrogen Source for Single Atom Cobalt-Catalyzed Wacker-Type Oxidation. *Catal. Sci. Technol.*, **2020**, *10*, 2769–2773.
[254] Zhang, T.; Zhang, D.; Han, X.; Dong, T.; Guo, X.; Song, C.; Si, R.; Liu, W.; Liu, Y.; Zhao, Z. Preassembly Strategy To Fabricate Porous Hollow Carbonitride Spheres Inlaid with Single Cu–N3 Sites for Selective Oxidation of Benzene to Phenol. *J. Am. Chem. Soc.*, **2018**, *140*, 16936–16940.
[255] Deng, D.; Chen, X.; Yu, L.; Wu, X.; Liu, Q.; Liu, Y.; Yang, H.; Tian, H.; Hu, Y.; Du, P.; Si, R.; Wang, J.; Cui, X.; Li, H.; Xiao, J.; Xu, T.; Deng, J.; Yang, F.; Duchesne, P.N.; Zhang, P.; Zhou, J.; Sun, L.; Li, J.; Pan, X.; Bao, X. A Single Iron Site Confined in a Graphene Matrix for the Catalytic Oxidation of Benzene at Room Temperature. *Sci. Adv.*, **2015**, *1*, e1500462.
[256] Wu, K.; Zhan, F.; Tu, R.; Cheong, W.-C.; Cheng, Y.; Zheng, L.; Yan, W.; Zhang, Q.; Chen, Z.; Chen, C. Dopamine Polymer Derived Isolated Single-Atom Site Metals/N-Doped Porous Carbon for Benzene Oxidation. *Chem. Commun.*, **2020**, *56*, 8916–8919.
[257] Chen, Z.; Zhang, Q.; Chen, W.; Dong, J.; Yao, H.; Zhang, X.; Tong, X.; Wang, D.; Peng, Q.; Chen, C.; He, W.; Li, Y. Single-Site AuI Catalyst for Silane Oxidation with Water. *Adv. Mater.*, **2018**, *30*, 1704720.
[258] Ledendecker, M.; Pizzutilo, E.; Malta, G.; Fortunato, G.V.; Mayrhofer, K.J.J.; Hutchings, G.J.; Freakley, S.J. Isolated Pd Sites as Selective Catalysts for Electrochemical and Direct Hydrogen Peroxide Synthesis. *ACS Catal.*, **2020**, *10*, 5928–5938.
[259] Guo, Z.; Xie, Y.; Xiao, J.; Zhao, Z.-J.; Wang, Y.; Xu, Z.; Zhang, Y.; Yin, L.; Cao, H.; Gong, J. Single-Atom Mn–N4 Site-Catalyzed Peroxone Reaction for the Efficient Production of Hydroxyl Radicals in an Acidic Solution. *J. Am. Chem. Soc.*, **2019**, *141*, 12005–12010.
[260] Xu, J.; Zheng, X.; Feng, Z.; Lu, Z.; Zhang, Z.; Huang, W.; Li, Y.; Vuckovic, D.; Li, Y.; Dai, S.; Chen, G.; Wang, K.; Wang, H.; Chen, J.K.; Mitch, W.; Cui, Y. Organic

Wastewater Treatment by a Single-Atom Catalyst and Electrolytically Produced H2O2. *Nat. Sustainablility*, **2020**, 1–9.
[261] Huang, L.; Chen, J.; Gan, L.; Wang, J.; Dong, S. Single-Atom Nanozymes. *Sci. Adv.*, **2019**, *5*, eaav5490.
[262] Lin, Z.; Zheng, L.; Yao, W.; Liu, S.; Bu, Y.; Zeng, Q.; Zhang, X.; Deng, H.; Lin, X.; Chen, W. A Facile Route for Constructing Cu–N–C Peroxidase Mimics. *J. Mater. Chem. B*, **2020**, *8*, 8599–8606.
[263] Lei, G.; Tong, Y.; Shen, L.; Liu, F.; Xiao, Y.; Lin, W.; Zhang, Y.; Au, C.; Jiang, L. Highly Active and Sulfur-Resistant Fe–N4 Sites in Porous Carbon Nitride for the Oxidation of H2S into Elemental Sulfur. *Small*, **2020**, *16*, 2003904.
[264] Wang, J.; You, R.; Zhao, C.; Zhang, W.; Liu, W.; Fu, X.-P.; Li, Y.; Zhou, F.; Zheng, X.; Xu, Q.; Yao, T.; Jia, C.-J.; Wang, Y.-G.; Huang, W.; Wu, Y. N-Coordinated Dual-Metal Single-Site Catalyst for Low-Temperature CO Oxidation. *ACS Catal.*, **2020**, *10*, 2754–2761.
[265] Zhou, P.; Hou, X.; Chao, Y.; Yang, W.; Zhang, W.; Mu, Z.; Lai, J.; Lv, F.; Yang, K.; Liu, Y.; Li, J.; Ma, J.; Luo, J.; Guo, S. Synergetic Interaction between Neighboring Platinum and Ruthenium Monomers Boosts CO Oxidation. *Chem. Sci.*, **2019**, *10*, 5898–5905.
[266] Kyriakou, G.; Boucher, M.B.; Jewell, A.D.; Lewis, E.A.; Lawton, T.J.; Baber, A.E.; Tierney, H.L.; Flytzani-Stephanopoulos, M.; Sykes, E.C.H. Isolated Metal Atom Geometries as a Strategy for Selective Heterogeneous Hydrogenations. *Science*, **2012**, *335*, 1209–1212.
[267] Gaudry, É.; Chatelier, C.; Loffreda, D.; Kandaskalov, D.; Coati, A.; Piccolo, L. Catalytic Activation of a Non-Noble Intermetallic Surface through Nanostructuration under Hydrogenation Conditions Revealed by Atomistic Thermodynamics. *J. Mater. Chem. A*, **2020**, *8*, 7422–7431.
[268] Greiner, M.T.; Jones, T.E.; Beeg, S.; Zwiener, L.; Scherzer, M.; Girgsdies, F.; Piccinin, S.; Armbrüster, M.; Knop-Gericke, A.; Schlögl, R. Free-Atom-like d States in Single-Atom Alloy Catalysts. *Nat. Chem.*, **2018**, *10*, 1008–1015.
[269] Maroun, F.; Ozanam, F.; Magnussen, O.M.; Behm, R.J. The Role of Atomic Ensembles in the Reactivity of Bimetallic Electrocatalysts. *Science*, **2001**, *293*, 1811–1814.
[270] Gao, F.; Wang, Y.; Goodman, D.W. CO Oxidation over AuPd(100) from Ultrahigh Vacuum to Near-Atmospheric Pressures: The Critical Role of Contiguous Pd Atoms. *J. Am. Chem. Soc.*, **2009**, *131*, 5734–5735.
[271] Ward, T.; Delannoy, L.; Hahn, R.; Kendell, S.; Pursell, C.J.; Louis, C.; Chandler, B.D. Effects of Pd on Catalysis by Au: CO Adsorption, CO Oxidation, and Cyclohexene Hydrogenation by Supported Au and Pd–Au Catalysts. *ACS Catal.*, **2013**, *3*, 2644–2653.
[272] Luneau, M.; Shirman, T.; Filie, A.; Timoshenko, J.; Chen, W.; Trimpalis, A.; Flytzani-Stephanopoulos, M.; Kaxiras, E.; Frenkel, A.I.; Aizenberg, J.; Friend, C.M.; Madix, R.J. Dilute Pd/Au Alloy Nanoparticles Embedded in Colloid-Templated Porous SiO2: Stable Au-Based Oxidation Catalysts. *Chem. Mater.*, **2019**, *31*, 5759–5768.
[273] Ouyang, L.; Da, G.; Tian, P.; Chen, T.; Liang, G.; Xu, J.; Han, Y.-F. Insight into Active Sites of Pd–Au/TiO2 Catalysts in Hydrogen Peroxide Synthesis Directly from H2 and O2. *J. Catal.*, **2014**, *311*, 129–136.
[274] Zhang, H.; Watanabe, T.; Okumura, M.; Haruta, M.; Toshima, N. Catalytically Highly Active Top Gold Atom on Palladium Nanocluster. *Nat. Mater.*, **2012**, *11*, 49–52.

[275] Sun, J.; Han, Y.; Fu, H.; Qu, X.; Xu, Z.; Zheng, S. Au@Pd/TiO2 with Atomically Dispersed Pd as Highly Active Catalyst for Solvent-Free Aerobic Oxidation of Benzyl Alcohol. *Chem. Eng. J.*, **2017**, *313*, 1–9.